Atlantic Multidecadal Oscillation and Northern Hemisphere's climate variability

By **Marcia Glaze Wyatt**[1], **Sergey Kravtsov**[2], **and Anastasios A. Tsonis**[2]

27 March 2011

Submitted to *Climate Dynamics*

Abstract Proxy and instrumental records reflect a quasi-cyclic 50-to-80-year climate signal across the Northern Hemisphere, with particular presence in the North Atlantic. Modeling studies rationalize this variability in terms of intrinsic dynamics of the Atlantic Meridional Overturning Circulation influencing distribution of sea-surface-temperature anomalies in the Atlantic Ocean; hence the name Atlantic Multidecadal Oscillation (AMO). By analyzing a lagged covariance structure of a network of climate indices, this study details the AMO-signal propagation throughout the Northern Hemisphere via a sequence of atmospheric and lagged oceanic teleconnections, which the authors term the "stadium wave". Initial changes in the North Atlantic temperature anomaly associated with AMO culminate in an oppositely signed hemispheric signal about 30 years later. Furthermore, shorter-term, interannual-to-interdecadal climate variability alters character according to polarity of the stadium-wave-induced prevailing hemispheric climate regime. Ongoing research suggests mutual interaction between shorter-term variability and the stadium wave, with indication of ensuing modifications of multidecadal variability within the Atlantic sector.

[1] *Corresponding author address*: Department of Geologic Sciences, CIRES/INSTAAR, Benson Earth Sciences Building, University of Colorado-Boulder, Boulder, CO 80309, e-mail: marciawyatt@earthlink.net

[2] Department of Mathematical Sciences, Atmospheric Sciences Group, University of Wisconsin-Milwaukee, Milwaukee, WI 53201-0413, USA

Results presented here support the hypothesis that AMO plays a significant role in hemispheric and, by inference, global climate variability, with implications for climate-change attribution and prediction.

Keywords Climate indices · Teleconnections · AMO · NAO · ENSO · PDO

1 Introduction

A pressing challenge for climate science in the era of global warming is to better distinguish between climate signals that are anthropogenically forced and those that are naturally occurring at decadal and longer timescales. Identifying the latter is essential for assessing relative contributions of each component to overall climate variability.

Multi-century proxy records reflect the signature of such a low-frequency climate signal, paced at a typical timescale of 50 to 80 years, with pronounced presence in the North Atlantic (Stocker and Mysak 1992; Mann et al. 1995; Black et al. 1999, Shabalova and Weber 1999; Delworth and Mann 2000; Gray et al. 2004). A similar signature has been detected in the instrumental record (Folland et al. 1986; Kushnir 1994; Schlesinger and Ramankutty 1994; Mann and Park 1994, 1996; Enfield and Mestas-Nuñez 1999; Delworth and Mann 2000; Zhen-Shan and Xian 2007). Modeling studies, with divergent results dependent upon model design (Delworth et al. 2007; Msadek et al. 2010a, 2010b), qualitatively support this pattern and tempo of variability in terms of the Atlantic Meridional Overturning Circulation's (AMOC) influencing redistribution of sea-surface-temperature (SST) anomalies in the Atlantic Ocean (Delworth and Mann 2000; Dong and Sutton 2002; Latif et al. 2004; Knight et al. 2005). Observed multidecadal SST variability in the North Atlantic Ocean, believed consequent of variability in the AMOC, has been termed the Atlantic Multidecadal Oscillation (AMO: Kerr 2000; Enfield et al. 2001).

AMO significantly impacts climate in North America and Europe (Enfield et al. 2001, Sutton and Hodson 2005, Knight et al. 2006; Pohlmann et al. 2006). In fact, its influence may have a global character; a suite of studies have addressed bits and pieces of requisite interactions (Dong and Sutton 2002, 2007; Dima and Lohmann 2007; Grosfeld et al. 2008; Sutton and Hodson 2003, 2005, 2007; Sutton et al. 2003; Timmermann et al. 2007; Zhang and Delworth 2005, 2007; Zhang et al. 2007; Polyakov et al. 2009).

Atlantic-related multidecadal variability reflected in geographically diverse proxy and instrumental records, combined with an abundance of numerical studies that link the hemispheric climate signal to AMO-related North Atlantic variability, guide our hypothesis and motivate our present investigation. We endeavor to put these previous results into perspective through use of a statistical methodology that characterizes Northern Hemispheric multidecadal climate variability and provides rigorous statistical bounds on the associated uncertainties. Emergent is a picture of a climate signal propagating from the North Atlantic throughout the Northern Hemisphere via a sequence of atmospheric and lagged oceanic teleconnections. We term this signal the "stadium wave". The stadium wave is examined here both in terms of its role in generating a multidecadally varying hemispheric climate signature and in its relationship with interannual-to-interdecadal climate variability.

Our philosophical approach, data sets, and analysis methods are described in section 2. Section 3 contains the results of our analyses. Section 4 summarizes our work and discusses potential mechanisms underlying the stadium wave.

2 Approach, data sets and methods

2.1 Approach

Our strategy was to evaluate collective behavior within a network of climate indices. Considering index networks rather than raw 3-D climatic fields is a relatively novel approach that has its own advantages — such as potentially increased dynamical interpretability, along with apparent increase of signal-to-noise ratio, and enhanced statistical significance — at the expense of detailed phenomenological completeness. In particular, the climate indices may represent distinct subsets of dynamical processes — tentatively, "climate oscillators" — that might, however, exhibit various degrees of coupling (Tsonis et al. 2007). As these indices also pertain to different geographical regions, we directly address the question of the global multidecadal teleconnections. Using fairly standard multivariate statistical tools, we aim to characterize dominant mode of climate co-variability in the Northern Hemisphere and provide rigorous estimates of its statistical significance, namely: What are the chances that the low-frequency alignment of various regional climatic time series, alluded to in an impressive suite of previous climate studies (see section 1), is, in fact, random? Our methodology allows us to give a quantitative answer to this question. Furthermore, objective filtering of the multidecadal signal provides a clearer picture of higher-frequency climate variability and its possible multi-scale interactions within the climate system.

2.2 Data sets

Insights gained from extensive literature review regarding proxy records, instrumental data, and climate-model studies; completeness of data sets throughout the 20th century;

97 and preliminary examination of linearly detrended 30-year (should be 13-year) smoothed
98 index-anomaly time series (not shown), collectively prompted our choice to use two
99 subsets of climate indices to address our hypotheses. A main set of eight indices focused
100 on the role played by the stadium-wave teleconnection sequence in the evolution of the
101 multidecadal hemispheric climate signal. Seven complementary indices were then used to
102 generate a larger fifteen-member network (**Table 1**)[3]; the goals here were to (i) check the
103 robustness of our results to the choice of index subset; (ii) to paint a more complete
104 picture of multidecadal variability; and (iii) to investigate more fully the role of higher-
105 frequency behavior in relation to multidecadal stadium-wave propagation.

106 The original subset of eight indices contained the Northern Hemisphere area-
107 averaged surface temperature (NHT), the Atlantic Multidecadal Oscillation (AMO),
108 Atmospheric-Mass Transfer anomaly (AT), the North Atlantic Oscillation (NAO), El
109 Niño/Southern Oscillation (NINO3.4), the North Pacific Oscillation (NPO), the Pacific
110 Decadal Oscillation (PDO), and the Aleutian Low Pressure (ALPI) indices. The
111 complementary set of seven indices used to generate our expanded network included: the
112 North Pacific Gyre Oscillation (NPGO), ocean-heat-content anomalies of the upper 700
113 and 300 meters in the North Pacific Ocean (OHC700 and OHC300), the Pacific North
114 American (PNA) pattern, the Western Pacific (WP) pattern, the Pacific Meridional Mode
115 (PMM), and the Atlantic Meridional Mode (AMM) indices. In order to maintain
116 consistency with previous studies to which we compare our results, some of the analyses
117 below will also include another ENSO index, the NINO3 index based on the Kaplan et al.
118 (1998) sea-surface temperature data set. All of these indices have been used extensively

[3] The time series of the indices used is later shown in Fig. 7, in terms of their decomposition into multidecadal signal and remaining higher-frequency variability.

in previous studies and highlight distinctive subsets of climatic processes; see Table 1 for references and brief description of each index.

We focused on boreal winter — the period when seasonally sequestered SST anomalies re-emerge (Alexander and Deser 1995), thereby enhancing conditions for potential oceanic–atmospheric coupling. Allied with this goal, the majority of our indices represent the months DJFM. Exceptions include AMO, AT, and OHC, which are annual; this due to logistics of data acquisition, with expectation of minimal impact on results.

Gapless time series of all eight primary indices over the 20th century period (1900–1999) are available[4]. Records are less extensive for the complementary set of seven indices — available for only the second half of the 20th century. To in-fill missing values, we used a covariance-based iterative procedure (Schneider 2001; Beckers and Rixen 2003; Kondrashov and Ghil 2008) described in section 2.3.2. This procedure assumes co-variability-statistics between continuous and gapped indices remain uniform throughout the century. Therefore, some detected relationships among reconstructed indices in the first half of the 20th century may partially reflect statistical co-dependencies of late 20th century indices. We guard against interpreting such relationships in dynamical ways (see section 3.2). Prior to analysis, all raw indices were linearly detrended and normalized to unit variance.

[4] This was one of the reasons to consider these as our primary subset.

2.3 Methodology

2.3.1 Spatiotemporal filtering and climate-signal identification

Compact description of dominant variability implicit in the multi-valued index time series described in section 2.3 was accomplished by disentangling the lagged covariance structure of this data set via Multichannel Singular Spectrum Analysis (M-SSA: Broomhead and King 1986; Elsner and Tsonis 1996; Ghil et al. 2002). M-SSA is a generalization of the more widely used Empirical Orthogonal Function (EOF; Preisendorfer 1988) analysis. M-SSA excels over EOF analysis in its ability to detect lagged relationships characteristic of propagating signals and has been used extensively to examine various climatic time series (Vautard and Ghil 1989; Ghil and Vautard 1991; Vautard et al. 1992; Moron et al. 1998; Ghil et al. 2002 and references therein).

M-SSA is, in fact, EOF analysis applied to an extended time series, generated from the original time series, augmented by M lagged (shifted) copies thereof. In M-SSA terminology, each of the multivalued index time series (e.g., AMO, NAO, etc.) is referred to as a channel. Because each multivalued index time series represents a spatial region, eigenfunctions of this extended lagged covariance matrix provide spatiotemporal filters, which define modes that optimally describe lagged co-variability of the original multivariate data set — analogous to EOFs optimally describing zero-lag co-variability.

M-SSA modes are represented in the original index space by their reconstructed components (RC). Each RC is effectively the narrow-band filtered version of an original multivariate time series, whose filters are related to coefficients (EOF weights) of M-SSA decomposition of the time series under consideration. In contrast to principal components (PCs) of EOF analysis, RCs are not mutually orthogonal, but their sum across all M-SSA

modes is identical to the original time series. We identify leading M-SSA modes with our climate signal and use the sum of their RCs to visualize variability associated with this climate signal.

2.3.2 Treatment of missing data

As mentioned in section 2.2, records are complete for the eight indices in the original subset, yet are limited for the seven indices comprised in our complementary set — these are available only since about 1950. M-SSA can be used to infill incomplete data sets; hence, we applied this technique to our extended set of 15 climate indices. The imputation procedure was developed in Beckers and Rixen (2003) and Kondrashov and Ghil (2008); it is a simpler version of the method proposed by Schneider (2001). At the initial stage, missing values of each index were replaced by this index's time mean, which was computed over available data points. Anomalies associated with this stage's "climatology" were formed, followed by application of M-SSA to the resulting anomaly field. Time series in channels with missing data were then reconstructed (data at points with actual data were not changed). Only the first N M-SSA RCs were retained, where N was chosen to correspond to the number of modes that account for a certain fraction (we use 90%) of the full data set's variability. Remaining modes were regarded as noise and did not participate in the reconstruction. At the next iteration, the climatology based on a newly computed index time series was subtracted from the corresponding indices. The procedure was repeated until convergence, i.e., until in-filled data values stop changing within 10% of their standard error. Results of the data infilling were insensitive to the M-SSA window used, for window sizes M=10, 20, 30, and 40.

We stress our caution in interpretation of statistical relationships found between in-filled indices in the first part of the 20th century. These relationships will be considered real only if their counterparts exist in the late 20th century.

2.3.3 Assessing statistical significance of stadium-wave-related cross-correlations

We tested statistical significance of M-SSA identified multidecadal modes (section 3.1) and that of cross-correlations between interannual-to-interdecadal climate indices (section 3.2) using two different stochastic models. The first model is a red-noise model fitted independently to each index considered. It has the form

$$x^{n+1} = ax^n + \sigma w, \qquad (1)$$

where x^n is the simulated value of a given index at time n; x^{n+1} is its value at time $n+1$; w is a random number drawn from the standard normal distribution with zero mean and unit variance, while parameters a and σ are computed by linear regression. Model (1) produces surrogate time series characterized by the same lag-1 autocorrelation as the original (one-dimensional) data. However, by construction, true cross-correlations between surrogate time series of different indices are zero at any lag. Nonzero cross-correlations between these time series are artifacts of sampling due to finite length of the time series considered. Observed correlation between any pair of actual time series is considered to be statistically significant only if it lies outside of the envelope of correlation values predicted by multiple surrogate simulations of this pair generated by model (1).

The second model is a multivariate, two-level extension of model (1) [Penland 1989, 1996; Penland and Ghil 1993; Kravtsov et al. 2005]. Construction of this second

model was based on 15-index *anomalies with respect to the multidecadal signal* in order to concentrate on interannual-to-interdecadal, rather than multidecadal, variability. The model produces random realizations of the 15-valued climate-index anomalies with lag 0, 1, and 2-yr covariance structure (including cross-correlations between the indices), which is statistically indistinguishable from the observed covariance structure. We used this model to test if cross-correlations between members of our climate network, *computed over various sub-periods of the full time series* (see sections 2.3.4 and 3.2.2), exceeded sampling thresholds quantified by this model's surrogate realizations. In other words, we looked into non-stationary relationships between pairs of indices characterized by stronger-than-normal cross-index synchronization, depending on time segment analyzed. Our detailed methodology for this part of analysis is summarized in section 2.3.4.

2.3.4 Testing for abnormal short-term synchronizations within the climate network

Definition of synchronization measure: Network connectivity. We first computed absolute values of cross-correlations between pairs of observed indices among all 15 members of our climate network over a 7-yr-wide sliding window[5]. This window size was chosen as a compromise between maximizing the number of degrees of freedom in computing cross-correlations, while minimizing the time segment allotted in order to capture the characteristically brief duration of synchronization episodes (Tsonis et al. 2007; Swanson and Tsonis 2009). This procedure resulted in 100-yr time series for each of the 105 cross-correlations among all possible pairs of the 15 indices; for each of the 100 years, we stored these cross-correlation values in the lower triangular part of the

[5] The M-SSA-defined multidecadal signal was subtracted from the indices prior to computing cross-correlations.

232 15×15 cross-correlation matrix, with all other elements of this matrix being set to zero.
233 We then defined the *connectivity* of our climate index network for a given year as the
234 leading singular value of the Singular Value Decomposition (SVD; Press et al. 1994) of
235 the above cross-correlation matrix, normalized by the square root of the total number of
236 nonzero cross-correlations in this matrix (which equaled to 105 for the case of the full 15-
237 index set). The connectivity defined in this way described a major fraction (typically
238 larger than 80%; not shown) of the total squared cross-correlation within the network of
239 climate indices, while providing a more robust measure of synchronization than the raw
240 sum of squared correlations (cf. Swanson and Tsonis 2009). The maxima of connectivity
241 time series defined local episodes of the climate network synchronization.

242 **Identification of synchronizing subsets.** Not all members of the climate network
243 contribute equally to various synchronization episodes. To identify index subsets that
244 maximize synchronization measure during such episodes, we employed the following re-
245 sampling technique. We randomly drew a subset of K different indices (K varied from 6
246 to 10) from the full set of 15 indices and computed 100-yr long connectivity time series
247 based on this subset. We repeated this procedure 10,000 times, producing 10,000 100-yr
248 long connectivity time series. We then identified indices and years for which the
249 connectivity value, based on at least one subset including this index, exceeded 95^{th} and
250 99^{th} percentiles of all connectivities that were based on the entire combined set of (100
251 yr) $\times$(10,000 samples) surrogate connectivity values.

252 **Statistical significance of synchronizations.** To estimate statistical significance
253 of synchronizations, we produced 1000 random realizations of the 15-valued climate-
254 index time series using the second stochastic model described in section 2.3.3. While

255 these surrogates mimic actual observed indices in the overall (climatological) covariance
256 structure, they, by construction, are mathematically unaware of the magnitude and/or
257 phasing of the multidecadal signal that was subtracted from the original data.

258 Connectivity time series for surrogate indices were then computed for each of the
259 1000 realizations in the same way as for the original data. The 95th percentile of surrogate
260 connectivity for each year defines the 5% *a priori* confidence levels. These levels should
261 be used if one tests for some pre-defined years in the climate record being characterized
262 by statistically significant synchronizations.

263 If no such a priori reasons exist, one has to use *a posteriori* confidence levels,
264 which can be defined as follows. For each synthetic realization, we determine the
265 maximum value of connectivity *over the entire 100-yr period*; repetition of this procedure
266 for all stochastic realizations results in 1000 values of maximum surrogate connectivities.
267 The 95th percentile of these maximum surrogate connectivities gives the 5% *a posteriori*
268 confidence level for rejection of the null hypothesis stating that connectivity for each year
269 is statistically the same as its true stationary value based on the correlation matrix
270 computed over the entire 100-yr period.

271

272 **3 Results**

273 **3.1 Multidecadal "stadium wave"**

274 Individual and cumulative variances of M-SSA modes for the main set of eight climate
275 indices are shown in **Figs. 1**a, b. The leading pair of modes is well separated from the
276 others according to the North et al. (1982) criterion. For the latter estimation, we have
277 computed the number of effective temporal degrees of freedom N^* in our data set using

the Bretherton et al. (1999) formula $N^* = N(1-r^2)/(1+r^2)$, where N=100 is the length of the time series, and $r \approx 0.65$ is the maximum lag-1 autocorrelation among our set of eight indices. We will hereafter identify this statistically significant leading M-SSA pair with our climate "signal." This dominant M-SSA pair *is unlikely to be due to random sampling of uncorrelated red-noise processes*, since it accounts for a substantially larger variance [exceeding the 97th percentile – upper dashed line in panel (a)] of the corresponding surrogate spectra generated by model (1).

Normalized RCs corresponding to joint M-SSA modes 1 and 2 are shown in **Fig. 2**; note that the reconstructions of *negative* NHT and AMO indices are displayed. Visual inspection of these RCs indicates they are dominated by a multidecadal climate signal with the time scale of about 50–80 yr. Maximum-entropy spectral analysis (Press et al. 1994) of each of these RCs centers on the period of the broadband variability identified at about 64 yr, indicative of long time scales associated with ocean dynamics.

Our climate signal accounts for a substantial fraction of variance in several indices: NHT, AMO, PDO, and AT (see the values corresponding to zero low-pass filter time scale in **Fig. 3a**). This latter manifestation (AT) demonstrates a clear atmospheric response to ocean-induced multidecadal climate variations. On the other hand, fractional weakness of the multidecadally varying climate signal exists in NAO, ALPI, NPO, and NINO3.4; these are dominated by shorter-term fluctuations. Despite dominance of higher frequency behavior in the NAO, ALPI, NPO, and NINO3.4 modes, M-SSA still identifies within these indices a statistically significant, coherent multidecadal signal.

To demonstrate robustness of these results, we repeated M-SSA analysis using the running-mean boxcar low-pass filtered indices. We used three filters, with sliding

301 window sizes of 10, 20, and 30 years. Ends of the data series are processed using shorter-
302 filter-size running means and one-sided (or asymmetric) filters. Fraction of variance
303 accounted for by the leading M-SSA pair of low-pass filtered data generally increases
304 with scale of low-pass filter, the fractional increase of variance being most dramatic for
305 ALPI, NPO, NAO, and NINO3.4 (Fig. 3a). Normalized RCs of the leading M-SSA mode
306 of low-pass filtered indices are close to their counterparts obtained via M-SSA analysis of
307 raw indices. Fig. 3b shows this behavior in NAO. Note boxcar low-pass filtering is
308 intrinsically characterized by a large phase error. This error is not entirely eliminated by
309 M-SSA time–space covariance-based filtering, explaining shifts between the maxima and
310 minima of filtered and raw RCs in Fig. 3b.

311 Figure 3b also illustrates well the distinction between M-SSA spatiotemporal
312 filtering and time filtering, underscoring the former's advantage in analyzing climate
313 data. Geophysical time series are typically characterized by presence of noise with
314 substantial power in the low-frequency portion of the spectrum — the so-called red noise.
315 Low-pass time filtering of a synthetic mixture of quasi-periodic time series with a strong
316 red-noise component may erroneously reflect spurious low-frequency variability that has
317 little to do with the shape of the actual quasi-periodic signal used to construct this time
318 series. On the other hand, if the quasi-periodic signal is characterized by a coherent
319 spatial structure that is distinct from noise, and if multivariate time series representing
320 geographically diverse indices possessing this signal are available, separation of signal
321 from noise is more robust (see Ghil et al. 2002 for further details). Note M-SSA
322 reconstruction of low-pass filtered NAO index in Fig. 3b (light solid line) does not follow
323 exactly excursions of the original low-pass filtered NAO index (heavy solid line).

Deviations from purely temporal filtering reflect corrections resulting from M-SSA, which relies on cross-index lagged correlations of the dominant multidecadal signal.

To confirm a truly multivariate nature of the leading M-SSA signal, we employed the following bootstrap procedure. We randomly generated multiple (~15,000) combinations of the eight primary indices and applied M-SSA to each randomly assembled set, resulting in multiple sets of eight-valued RC time series — in some cases with certain indices being repeated, and others being omitted. For each of the eight indices, this procedure resulted in 10,000 sets of RC time series corresponding to leading M-SSA pairs of random index sets. Any statistical characteristic based on RCs of the original index set can also be computed for surrogate sets. The latter estimates can be used to assess the expected spread of statistical quantities computed. For example, the bootstrap-based estimate of dominant timescale of the leading M-SSA signal produces the mean value of 63 yr, with the standard uncertainty of ±5 yr and 95% confidence interval close to twice the standard uncertainty. These estimates are thus consistent with results of the original eight-index analysis. *Robustness of bootstrap-based M-SSA reconstructions highlights lagged co-variability among the entire set of eight indices; the leading M-SSA signal is not "dominated" by the variability in a particular M-SSA channel (say, NHT or AMO).*

It is apparent from Fig. 2 that the climate-signal indices are correlated at nonzero lags, except for the normalized RCs 6 (NPO) and 7 (PDO), which turned out to be virtually identical. We objectively determined the lead–lag relationships between the RCs using the cross-correlation analysis (not shown), which unambiguously identifies, based on maximum cross-correlation, the order of RCs in the "stadium wave" propagation

across the phase space of the reconstructed climate indices. The phase of each RC in the stadium-wave sequence was computed by least-square fitting two-predictor time series $\{\sin(2\pi t/64),\cos(2\pi t/64)\}$, with t changing from 0 to 100, to each of the RCs. The following phase shifts between the "adjacent" RC pairs resulted:

–NHT →(4 yr)→ –AMO →(7 yr)→ AT →(2 yr) → NAO →(5 yr)→ NINO3.4 (3 yr)→ NPO/PDO →(3 yr)→ ALPI →(8 yr)→ NHT →(4yr)→ AMO → (7 yr)→ –AT →(2 yr)→ –NAO →(5 yr)→ –NINO3.4→ (3 yr)→ –NPO/PDO→ (3 yr)→ –ALPI→ (8 yr)→ –NHT.

This "stadium wave" is summarized as a Hoffmuller diagram in **Fig. 4**. The complete cycle of the stadium wave has naturally a period of 64 yr, and a bootstrap-based standard uncertainty of ±5 yr. The bootstrap-based estimates of the above lags and their uncertainties are listed in **Table 2**. Note that the fractional uncertainties vary considerably from one transition leg to another, due mainly to differences in mean duration of various transitions in the presence of fairly uniform absolute uncertainty. This describes the case for all but the –NHT→–AMO and –AMO → +AT transitions, which involve indices strongly dominated by low-frequency anomalies. Uncertainty of lag-time between these indices is smaller than that associated with index pairs involving noisier raw indices.

M-SSA results for the extended data set support those of the original stadium-wave analysis. Leading M-SSA modes 1 and 2 describe the multidecadal stadium wave, with no modification of phase relationships between the original eight indices (Fig. 4 and **Fig. 5**). While all 15 indices reflect the dominant multidecadal signature, a stronger high-frequency component characterizes most of the seven complementary indices, rendering their fractional variance of the stadium-wave signal weak. Only those with strong

fractional variance — PNA and OHC300/700 — are displayed in the Hoffmuller diagram in Fig. 4. OHC700 exhibits the strongest fractional variance among the trio from the complementary indices, with a strong multidecadal component nearly in phase with that of the AT index. OHC300, on the other hand, exhibits a much lower fractional variance and its phasing is close to the NAO and NINO3.4 multidecadal signals. These observations invite speculation that ocean-heat-content variability at various depths within the subsurface North Pacific is governed by different dynamical processes related to indices within the stadium-wave network (see also discussion in section 4.2).

3.2 Interannual-to-interdecadal variability

3.2.1 Variability unrelated to the stadium wave

To extract a residual signal from our 15 indices, we subtract the multidecadal signal (**Fig. 6**, blue lines) associated with the stadium wave. This forms a network of climate indices (Fig. 6, red lines) that emphasizes higher-frequency, interannual-to-interdecadal climate variability. To study possible connections within this network, we first identify statistically significant (lagged) cross-correlations between index anomalies so computed (see **Table 3**). *A posteriori* significance levels were determined for each index pair using surrogate indices simulated by the red-noise model (1); see section 2.3.3. We computed maximum lagged correlations (using the entire 100-yr time series and over a range of all possible lags) for 100 sets of surrogate index time series, followed by sorting these correlations in ascending order, taking the 99^{th} sorted values as the 1% significance level.

Analysis results of high-frequency variability of the residual signal point to a Pacific-centered subset of indices — PNA, PDO, ALPI, NINO3.4, WP, NPO — whose

394 members exhibit behavior similar to one another (that is, they are correlated at zero or
395 one-year lags). Guided by this observation, we applied M-SSA to this select group of
396 indices as a way to verify suspected relationships among them and to more graphically
397 describe the cross-correlations between them. Relationships identified in cross-
398 correlation analysis are corroborated by M-SSA results (**Figs. 7** and **8**). In particular, we
399 find NINO 3.4 and NPO correlated at zero lag; although the low fractional variance of
400 NPO suggests caution regarding its degree of uncertainty. The same is true for WP (see
401 section 4.3). NINO3.4 and NPO lead others within this subset by one year, with the
402 typical time scale of variability being on the order of three to four years. Based on time
403 scale and spatial confinement, behavior of the Pacific-centered set has strong association
404 with ENSO. These results are not surprising or novel. However, they do demonstrate that
405 the network approach we took is sound, as it corroborates previous findings by other
406 researchers on ENSO teleconnections.

407 Another statistically significant cross-index relationship identified includes that
408 between OHC700 and OHC300, which is, of course, not unexpected given the similar
409 nature of the two indices. There is also the anti-correlation between the members of
410 PMM/NPGO pair. Both of the latter indices are dominated by interdecadal anomalies
411 (see Fig. 6). There is also a statistically significant positive simultaneous correlation
412 between the interdecadal anomalies of AMO and NHT indices, demonstrating that the
413 North Atlantic decadal-to-interdecadal SST anomalies directly explain a significant
414 fraction of the NHT decadal-to-interdecadal variability. Finally, the cross-correlation
415 analysis identifies substantial co-variability within the Atlantic-based index trio: AMM,

AMO, and NAO, thus suggesting interesting dynamical connections among various components of the coupled AMOC system.

3.2.2 Effects of the stadium wave on interannual-to-interdecadal climate anomalies

Next we wish to see if collective behavior of higher-frequency variability of the residual signal has a relationship with the stadium-wave multidecadal signal. This line of inquiry was motivated by work of Tsonis et al. (2007) and Swanson and Tsonis (2009). These authors identified five intervals within the 20th century during which certain climate indices abnormally synchronized — matching with strong statistical significance in both rhythm and phase of their interannual variability; the five intervals were centered at the years 1916, 1923, 1940, 1957, and 1976. Three of five synchronizations (1916, 1940, 1976) coincided with hemispheric climate-regime shifts, which were characterized by a switch between distinct atmospheric and oceanic circulation patterns, a reversal of NHT trend, and by an altered character of ENSO variability (intensity and dominant timescale of variability (Federov and Philander 2000; Dong et al. 2006; Kravtsov 2010, among others). As the authors had expected, based on synchronized chaos theory, these "successful" synchronizations (i.e., the ones preceding climate shifts) were accompanied by increased network coupling defined via the climate index network's phase-prediction measure. Two synchronizations *not* leading a climate-regime shift were *not* accompanied by increased network coupling. We observe here that the timing of the regime shifts has a multidecadal pace, consistent with the stadium wave; we are thus motivated to further explore synchronizations in our extended (compared to Tsonis et al.) climate network.

438 We first determine the years of abnormal synchronizations and synchronizing
439 subsets within the main 15-index set using the methodology described in section 2.3.4.
440 Results presented in **Fig. 9** identify five time bands characterized by high connectivity
441 values among the subsets of the full 15-index set; these bands are centered at years 1916,
442 1923, 1940, 1957 and 1976 — thus consistent with studies by Tsonis et al. Synchronizing
443 subsets comprise the following indices (based on the 99th percentile of re-sampled sub-
444 networks; see section 2.2.4): AMM, NAO, NPGO, PNA, WP, PDO for the 1916 subset;
445 AMO, AMM, NAO, NPGO, PNA, ALPI for the 1923 subset; AMO, AT, NAO, PNA,
446 PMM, ENSO, PDO, ALPI for the 1940 subset; PNA, ENSO, NPO, PDO, ALPI, NHT for
447 the 1957 subset; and AMO, AT, NAO, OHC700, OHC300, PNA, WP, PDO ALPI, NHT
448 for the 1976 subset. Connectivity time series computed for each subset exhibit
449 statistically significant maxima during corresponding time bands (**Fig. 10**). While the
450 statistical significance of connectivity maxima drops substantially if one accounts for
451 degrees of freedom associated with possibility of drawing multiple index subsets of a
452 given size from the full set of 15 indices, all of the connectivity maxima in Fig. 10 still
453 exceed the 5% *a priori* levels in this case (not shown). The use of *a priori* levels may, in
454 fact, be more appropriate for successful synchronization episodes, given the evidence for
455 regime shifts and predictions of synchronized chaos theory that rationalize expected
456 synchronizations preceding these shifts (Tsonis et al. 2007; Swanson and Tsonis 2009).
457 Our results here provide a more detailed picture of the 1916, 1940 and 1976
458 ("successful") synchronizations and expose differences between these three "successful"
459 and two "unsuccessful" episodes (i.e., 1923 and 1957) in terms of index membership of
460 corresponding synchronizing subsets. In particular, the 1957 episode is confined mostly

within the Pacific; while the Atlantic reflects a greater influence during the 1923 synchronization. Successful synchronizations tend toward a more symmetrical contribution from both the Atlantic and Pacific sectors and PNA participates in all synchronizations. Note that timing between successful synchronizations, shifts between alternating periods of enhanced and diminished interannual variance of ENSO and NAO (**Fig. 11**), and the stadium-wave tempo share similar pace, thus suggesting possible stadium-wave influence on synchronizations within the climate network.

In summary, while our research on the interrelationships between the multidecadal signal and higher-frequency variability continues, the above results suggest that the major synchronization episodes and regime shifts of interannual-to-decadal climate variability all over the world are paced by the multidecadal climate variations originating in the North Atlantic (see section 4).

4 Summary and discussion

4.1 Summary

We considered the Northern Hemisphere's climate variability in a network of well-known indices describing climatic phenomena all over the Northern Hemisphere (NH). Our network approach — via data compression to a subspace of dynamically and geographically distinct indices — provides means to establish rigorous estimates of uncertainty associated with multidecadal variability observed in the instrumental climate records and to address the question of how likely these observed multidecadal teleconnections are to be due merely to random sampling of uncorrelated red-noise time series. Multi-channel Singular Spectrum Analysis (M-SSA) of this network (Figs. 1–5)

484 identifies the dominant signal with a time scale of 50–80 yr, which propagates through
485 the phase space of the indices considered as the "stadium wave" (Fig. 4, Table 2). In
486 section 4.2 below, we interpret this stadium wave in terms of the sequence of atmospheric
487 and multi-year-lagged oceanic teleconnections originating from the Atlantic Multidecadal
488 Oscillation (AMO) — an extensively studied intrinsic oceanic mode associated with the
489 variability of Meridional Overturning Circulation (MOC). The stadium-wave propagation
490 is reflected in the NH area-averaged surface temperature signal, which explains, by
491 inference, at least a large fraction of the multidecadal non-uniformity of the observed
492 global surface temperature warming in the 20th century.

493 In section 3.2, we decomposed the climate indices into the stadium-wave
494 multidecadal and shorter-term residual variability (Fig. 6). The dominant residual signal
495 is the Pacific-centered suite of interannual ENSO teleconnections (Table 3 and Figs. 7
496 and 8). Results summarized in Table 3 also show that a major portion of the shorter-term
497 (with respect to the stadium wave time scale), decadal-to-interdecadal variations of NH
498 surface temperature (NHT) is directly related to the corresponding variability of the
499 North Atlantic sea-surface temperature (SST). In combination with the inferred
500 AMO/NHT stadium-wave connections, these findings imply that the North Atlantic SSTs
501 exert a strong influence on the hemispheric climate across the entire range of time scales
502 considered.

503 One of the most intriguing findings that came out of our analysis is the apparent
504 connection between the hemispheric climate regime induced by the stadium-wave
505 dynamics and the character of interannual climate variability. In particular, the pacing of
506 the stadium wave is consistent with the timing between the episodes of abnormal

synchronization of Atlantic/Pacific teleconnections (Figs. 9–11). The termination of these synchronization episodes coincided with hemispheric climate-regime shifts characterized by the switch of the climate regime from the one characterized by the high ENSO variance (pre-1939), to the one with low ENSO variance (1939–1976), and back to the high ENSO variance regime (post-1976); see Fig. 11. The NAO interannual variance exhibits similar multidecadal variability, as shown in Fig. 11, suggesting Pacific–Atlantic feedback.

Thus, results presented in this note suggest that AMO teleconnections, as captured by our stadium-wave, have implications for decadal-scale climate-signal attribution and prediction — both significant to the developing field of climate research.

4.2 Discussion: Stadium-wave's hemispheric propagation

Statistical results developed above describe only co-variability within the climate-index network, not causality. We interpret these results based on a wide variety of observational and modeling studies, which rationalize the existence of the multidecadal climate signal — Atlantic Multidecadal Oscillation (AMO) — that originates dynamically in the North Atlantic Ocean and propagates throughout the Northern Hemisphere via a suite of atmospheric and oceanic processes, or the stadium wave.

Inconsistent modeling results foil simple narrative, with dependency of the simulated low-frequency climate variability upon model configuration, initialization, and spatial resolution (Metzger and Hurlburt 2001; Yualeva et al. 2001; Kushnir et al. 2002; Kelly and Dong 2004; Minobe et al. 2008). Instrumental records, on the other hand, are short, and while they have been shown to reflect a multidecadal signature (Folland et al.

530 1986; Kushnir 1994; Schlesinger and Ramankutty 1994; Delworth and Mann 2000), their
531 direct interpretation is difficult. These collective challenges are mollified somewhat by
532 observations from proxy records (Mann et al. 1995, 1998; Black et al. 1999; Shabalova
533 and Weber 1999; Gray et al. 2004), which do indicate the tendency of a diverse collection
534 of paleo-climate indices to exhibit climate variability on a shared multidecadal cadence –
535 a finding similar to ours.

536 Despite caveats of model studies, their results are instructive in context of our
537 proposed stadium wave, describing potential mechanisms for climate-signal generation
538 and its subsequent hemispheric propagation. Hypotheses for AMO origin often find
539 common ground in the suspicion that AMOC plays a nontrivial role in generating and
540 setting the pace of the AMO. Many models produce intrinsic interdecadal and
541 multidecadal variability (Delworth et al. 1993; Delworth et al. 1997; Timmermann et al.
542 1998; Cubasch and Voss 2000; Delworth and Greatbatch 2000; Hilmer and Jung 2000;
543 Eden and Jung 2001; Shindell et al. 2001; Bryden et al. 2005; Getzlaff et al. 2005;
544 Delworth and Dixon 2006; Latif et al. 2004, 2006; Dima and Lohmann 2007; Vellinga
545 and Wu 2004; Delworth et al. 2007; Msadek et al. 2010), although mechanisms behind
546 the observed variations are still a matter of debate. Models with periodicities and boreal-
547 winter atmospheric projections closest to observation seem to require a deep or
548 interactive ocean (Knight et al. 2005; Msadek et al. 2010b), underscoring the
549 hypothesized AMO link to AMOC-related ocean dynamics.

550 The Atlantic SST Dipole — an index based on interhemispheric Atlantic SST
551 anomalies — is thought to reflect AMOC-forced SST fluctuations related to the AMO
552 (Black et al. 1999; Keenlyside et al. 2008). Motivated by this observation, we added the

553 dipole to our MSSA mix of indices. What we found was the SST-dipole-index RC
554 identical in phasing to that of the NHT RC. NHT leads AMO by about four years — and
555 so does AMOC, according to the SST Dipole proxy. We also experimented with the
556 addition of a paleo-proxy for the SST Dipole (*G.bulloides*; see Black et al. 1999) to our
557 MSSA collection of indices and found, once again, the phasing identical to the NHT RC.
558 Considering the collective evidence — the dipole phasing, paleo-proxy phasing, and
559 model studies, we suggest the AMOC indeed plays a significant role in generating the
560 AMO.

561 **The AMOC generated multidecadal SST signal and its relationship with the**
562 **overlying atmosphere:** Bjerknes (1964) argued that long-term top-of-the-atmosphere
563 radiative balance remains fairly constant and so is the total poleward heat transport
564 accomplished by ocean and atmosphere. Therefore, when one vehicle of poleward heat
565 transport weakens, the other strengthens to compensate, the phenomenon known as
566 "Bjerknes Compensation." Shaffrey and Sutton (2006) and Van der Swaluw et al. (2007)
567 showed via modeling studies that Bjerknes compensation is operative in the northern
568 North Atlantic Ocean, with maximum expression between 60ºN and 80ºN, on decadal
569 and longer time scales. Note that the AMO SST index reflects the ocean surface signature
570 of AMOC multidecadal variability and is thus not representative of the oceanic heat
571 transport, which may exhibit decadal delays with respect to SST due to oceanic
572 dynamical inertia (see, for example, Marshall et al. 2001a,b; Kravtsov et al. 2008, and
573 references therein). Consistent with this notion, our results find that the –AMO index
574 leads the AT index (related to atmospheric mass and heat transport) and NAO index
575 (related to atmospheric mass) by 7 and 9 yr, respectively. This implies that

oceanic/atmospheric heat transport has a minimum/maximum a few years after peak negative SST anomalies in the North Atlantic, with atmospheric transport causing NAO to peak shortly after. These timings are consistent with Msadek et al. (2010b).

Relationship of the multidecadal SST signal transmitted with the overlying atmosphere: Mechanisms behind the North Atlantic SST anomalies' influence on the overlying atmosphere on decadal-to-multidecadal time scales, as suggested by the above energy-balance considerations, remain the subject of extensive research. For example, Kelly and Dong (2004) and Dong and Kelly (2004) found that strong basin-scale westerlies in both the North Atlantic and North Pacific co-occur with anomalously high ocean heat content and strong negative heat flux (out of the ocean) in the western-boundary currents and their extensions (see also Hansen and Bezdek 1996; Sutton and Allen 1997, McCartney 1997; Marshall et al. 2001a). These results argue that there exists a positive, reinforcing feedback on SST anomalies through oceanic modification of overlying atmospheric circulation (Palmer and Sun 1985; Latif and Barnett 1994, 1996; Kushnir and Held 1996; Rodwell et al. 1999; Latif et al. 2000; Mehta et al. 2000; Robertson et al. 2000; Czaja and Frankignoul 2002; Wu and Gordon 2002; Sutton and Hodson 2003; Wu and Rodwell 2004; Xie 2004; Xie and Carton 2004). Note, however, that details of this response are sensitive to the location of the heat source with respect to the mid-latitude storm track (Peng et al. 1997; Peng and Whittaker 1999; Peng and Robinson 2001; Czaja and Marshall 2001; Peng et al. 2002; Nakamura et al. 2004; Xie et al. 2004; Minobe et al. 2008), with substantial inconsistencies among the models — see Kushnir et al. (2002) for a review and Msadek et al. 2010b.

598 **Generation of the hemispheric response: Atlantic–Pacific teleconnections:** A
599 variety of models with prescribed AMO-related SSTs show consistent hemispheric
600 response (Delworth et al. 1993; Kushnir 1994; Hakkinen 1999; Delworth and Mann
601 2000; Sutton and Hodson 2003; Sutton and Hodson 2005; Knight et al. 2006; Grosfeld et
602 al. 2007; Sutton and Hodson 2007). Longitudinal and latitudinal migrations of
603 atmospheric centers-of-action (COA) appear to govern circumpolar communication of
604 regionally generated climate signals (Kirov and Georgieva 2002; Polonsky et al. 2004;
605 Grosfeld et al. 2006; Dima and Lohmann 2007; Msadek et al. 2010b). Dominant direction
606 of wind flow across the entire range of longitudes (AT) and inter-basin connectivity
607 modify accordingly: Wang et al. (2007) find that COA migrations generate intervals
608 when climate patterns over the North Pacific and over the Eurasian continent upstream
609 are linked, as are regions downstream, via an enhanced PNA and an eastwardly extended
610 jet stream. During these time segments of enhanced circum-hemispheric stationary wave
611 patterns, ENSO influence on ALPI becomes secondary to mid-latitude dynamics (Wang
612 et al. 2007). Latitudinal shifts in atmospheric COAs — strongly influenced by NPO/WP
613 patterns (Sugimoto and Hanawa 2009; Frankignoul et al. 2011) — have also been shown
614 to influence interdecadal-scale migrations of western-boundary-current extensions
615 (oceanic-gyre frontal boundaries), with impact on western-boundary dynamics and air-
616 sea interaction (Kwon et al. 2010; Frankignoul et al. 2011). These sets of processes, after
617 accounting for interannual delays due to oceanic dynamical adjustment, rationalize the
618 sequence of the hemispheric and Pacific centered indices in our stadium wave.
619 Other proposed mechanisms for conveying an Atlantic-born climate signal to the
620 North Pacific include stability changes within the tropical thermocline (Dong and Sutton

2005; Dong et al. 2006; Zhang and Delworth 2005, 2007; Zhang et al. 2007; Timmermann et al. 2007) and latitudinal shifts of Intertropical Convergence Zones (ITCZ) (Vellinga and Wood 2002; Vellinga and Wu 2004; Vimont and Kossin 2007). Tropical Pacific multidecadal changes may further modify the North Pacific response to AMO via an atmospheric bridge (Lau and Nath 1994; Deser and Blackmon 1995; Zhang et al. 1996). All the while, the AMOC continues its quasi-oscillatory behavior; the related AMO teleconnection sequence evolves accordingly. Possibly the Pacific communicates back to the Atlantic via tropical connections; this hypothesis will be addressed in a future study.

4.3 Discussion: Interannual-to-interdecadal variability

Our results support the notion that higher-frequency variability, especially in the Pacific, is modified according to polarity of the multidecadal signal. A Pacific subset — PNA, PDO, ALPI, NINO3.4, WP, and NPO — thus becomes a focus for this multidecadally alternating interannual-to-interdecadal behavior (see Table 3 and Fig. 8). Perhaps striking is the comparatively low fractional variance displayed by the NPO and its upper-atmosphere counterpart — WP — both of which show significant correlation with NINO3.4. Potentially relevant to this conundrum is the observation of a non-stationary relationship between the NPO and ENSO (Wang et al. 2007), with ENSO-related signal in the ALPI strengthening and weakening at a multidecadal pacing and affecting the hemispheric interconnectedness of mid-latitude Pacific-centered indices, including NPO and WP.

643 Absent from our Pacific grouping are NPGO and PMM, which other studies have
644 linked to ENSO by way of NPO. Our results suggest a strong negative relationship
645 between higher-frequency behavior of NPGO and PMM, but not a significant relationship
646 between NPGO and either NINO3.4 or NPO, in contrast to some other studies (Di
647 Lorenzo et al. 2009; Alexander et al. 2010). This discrepancy may be due to differences
648 underpinning methods and data used. For example, different authors used different
649 versions of the NPO index (Di Lorenzo et al. 2008; Chhak et al. 2008; Ceballos et al.
650 2009; Di Lorenzo et al. 2009; and Di Lorenzo et al. 2010), with possibly large ensuing
651 differences in the NPO–NPGO correlation. The same is true for various versions of
652 ENSO related indices. Further potential explanations for our finding no significant
653 correlations between NPO and PMM, as well as ENSO and PMM, include the seasonal
654 dependence of these cross-correlations missed in our boreal-winter index analysis, and
655 likely nonlinearity of the ENSO–PMM connection (Vimont et al. 2001, 2003 a, b; Chiang
656 and Vimont 2004; Chang et al. 2007), which is not optimally described by linear
657 correlation measures.

658 In conclusion, dynamics presented above — potential mechanisms underlying
659 stadium-wave dynamics and related dynamics on interdecadal time scales — are topics of
660 active and controversial research, reliant upon technological leaps in data retrieval and
661 computer modeling to advance them toward consensus. We suggest momentum on these
662 investigations is building and that our statistical analysis is consistent with these
663 emerging hypotheses.

664

Acknowledgements We thank S. Minobe for a useful feedback on aspects of this study, and three anonymous reviewers for comments on an earlier version of the manuscript, which helped clarify the presentation. This research was supported by the Office of Science (BER), U. S. Department of Energy (DOE) grant DE-FG02-07ER64428, NSF grant ATM-0852459 (SK), and NSF grant AGS-0902564.

References

Alexander MA, Deser C (1995) A mechanism for the recurrence of wintertime midlatitude SST anomalies. J Phys Oceanogr 25: 122-137.

Beamish RJ, Neville CM, Cass AJ (1997) Production of Fraser River sockeye salmon (*Oncorhynchus nerka*) in relation to decadal-scale changes in the climate and the ocean. Canadian Journ Fish and Aquat Sci 56: 516-526.

Bell GD, Halpert MS (1995) Atlas of intraseasonal and interannual variability, 1986-1993. NOAA Atlas No. 12. Climate Prediction Center, NOAA/NWS/NMC, Washington D. C. Request copy via e-mail from Gerald Bell at wd52gb@hp32.wwb.noaa.gov

Beckers J, Rixen M (2003) EOF calculations and data filling from incomplete oceanographic data sets. J Atmos Ocean Technol 20: 1839–1856. doi: 10.1175/1520-0426(2003)

Biasutti MA, Giannini A (2006) Robust Sahel drying in response to late 20th century forcings. Geophys Res Lett 33: L11706. doi:10.1029/2006GL026067

Bjerknes J (1964) Atlantic air-sea interaction. Advances in Geophysics 10. Academic

689 Press: 1–82
690 Black D, Peterson LC, Overpeck JT, Kaplan A, Evans MN, Kashgarian M (1999) Eight
691 Centuries of North Atlantic Ocean Atmosphere Variability. Science 286: 1709-
692 1713. doi: 10.1126/science.286.5445.1709
693 Broomhead DS, King GP (1986) Extracting qualitative dynamics from experimental data.
694 Physica D 20: 217–236
695 Bretherton, C.S, Widmann M, Dymnikov VP, Wallace JM, Blade I (1999) The effective
696 number of spatial degrees of freedom of a time-varying field. J. Climate, 12:
697 1990–2009
698 Bryden H, Longworth HR, Cunningham SA (2005): Slowing of the Atlantic meridional
699 overturning circulation at 25°N. Nature 438: 655-657. doi:10.1038/nature04385
700 Cassou C, Deser C, Terray L, Hurrell JW, Drevillion M (2004): Summer Sea Surface
701 Temperature Conditions in the North Atlantic and Their Impact upon the
702 Atmospheric Circulation in Early Winter. J Climate 17: 3349-3363. doi:
703 10.1175/1520-0042(2004)
704 Cayan DR (1992) Latent and Sensible Heat Flux Anomalies over the Northern Oceans,
705 Driving the Sea Surface Temperature. J Phys Ocean 22: 859-881
706 Ceballos LI, Di Lorenzo E, Hoyos CD, Schneider N, Taguchi B (2009) North Pacific
707 Gyre Oscillation synchronizes climate fluctuations in the eastern and western
708 boundary systems. J Clim 22: 5163-5174.
709 Chang P, Zhang Li, Saravanan R, Vimont DJ, Chiang JCH, Link Ji, Seidel H, Tippett
710 MK (2007) Pacific meridional mode and El Niño-Southern Oscillation. Geophys
711 Res Lett 34. L16608. doi:10.1029/2007GL030302.

712 Chhak K, Di Lorenzo E (2007) Decadal variations in the California Current upwelling
713 cells. Geophys Res Lett 314: L14604. doi10.1029/2007GL030203.
714 Chiang JCH, Vimont D (2004) Analogous Pacific and Atlantic Meridional Modes of
715 Tropical Atmosphere-Ocean Variability. J. Climate 17: 4143-4158. doi:
716 10.1175/JCLI4953.1
717 Crowley TJ (2000) Causes of Climate Change Over the Past 1000 Years. Science 289:
718 270-277. doi: 10.1126/science.289.5477.270
719 Cubasch U, Voss R, Hergerl GC, Waszkewitz J, Crowley TJ (1997) Simulation of the
720 influence of solar radiation variations on the global climate with an ocean-
721 atmosphere general circulation model. Clim Dyn 13: 757-767
722 Cubasch U, Voss R (2000) The Influence of Total Solar Irradiance on Climate. Space
723 Science Rev 94: 185-198. doi: 10.1023/A:1026719322987
724 Czaja A, Frankignoul C (2002) Observed Impact of Atlantic SST Anomalies on the North
725 Atlantic Oscillation. J. Climate 15: 606-623
726 Czaja A, Marshall J (2001) Observations of Atmosphere-Ocean Coupling in the North
727 Atlantic. OJR Met. Soc. 27: 1893-1916. doi:10.1002/qj.49712757603
728 Danabasoglu G (2008) On Multidecadal Variability of the Atlantic Multidecadal
729 Overturning Circulation in the Community Climate System Model Version 3. J
730 Climate 21: 5524-5544. DOI: 10.1175/2008JCLI2019.1
731 Delworth TL, Dixon KW (2006) Have anthropogenic aerosols delayed a greenhouse gas-
732 induced weakening of the North Atlantic thermohaline circulation? Geophys Res
733 Lett 33: L02606. doi:10.1029/2005GL024980

734 Delworth TL, Greatbatch RJ (2000) Multidecadal Thermohaline Circulation Variability
735 Driven by Atmospheric Surface Flux Forcing. J Climate 13: 1481-1495
736 Delworth TL, Manabe S, Stouffer RJ (1993) Interdecadal Variations of the Thermohaline
737 Circulation in a Coupled Ocean-Atmosphere Model. J Climate 6: 1993-2011
738 Delworth TL, Manabe S, Stouffer RJ (1997) Multidecadal climate variability in the
739 Greenland Sea and surrounding regions: a coupled mode simulation. Geophys Res
740 Lett 24 (3) 96GL03927: 257-260
741 Delworth TL, Mann ME (2000) Observed and simulated multidecadal variability in the
742 Northern Hemisphere. Climate Dyn 16: 661–676. doi:10.1007/s003820000075
743 Delworth TL, Zhang R, Mann ME (2007) Decadal to centennial variability of the
744 Atlantic from observations and models. In: Past and Future Changes of the
745 Oceans Meridional Overturning Circulation: Mechanisms and Impacts,
746 Schmittner A, Chiang JCH, Hemming SR, Eds., Geophysical Monograph Series
747 173, American Geophysical Union, pp. 131–148
748 Deser C, Blackmon ML (1995) On the Relationship between Tropical and North Pacific
749 Sea Surface Temperature Variations. J. Climate 8: 1677-1680
750 Di Lorenzo E, Schneider N, Cobb KM, Franks PJS, Chhak K, Miller AJ, McWilliams JC,
751 Bograd SJ, Arango H, Curchitser E, Powell TM (2008) North Pacific Gyre
752 Oscillation links ocean climate and ecosystem change. Geophys Res Lett 35:
753 L08607. doi:10.1029/2007GL032838
754 Di Lorenzo E, Fiechter J, Schneider N, Miller AJ, Franks PJS, Bograd SJ, Moore A,
755 Thomas A, Crawford W, Pena A, Herman AJ (2009) Nutrient and salinity

decadal variations in the central and eastern North Pacific. Geophys Res Lett 36: L14601. doi:10.1029/2009GL038261.

Di Lorenzo E, Cobb KM, Furtado JC, Schneider N, Anderson BT, Bracco A, Alexander MA, Vimont DJ (2010) Central Pacific El Niño and decadal climate change in the North Pacific Ocean. Nature Geosci 3 (11): 762-765. doi10.1038/NGEO984.

Dima M, Lohmann G (2007) A Hemispheric Mechanism for the Atlantic Multidecadal Oscillation. J Climate 20: 2706-2719. doi:10.1175/JCL14174.1

Dong BW, Sutton RT (2002) Adjustment of the coupled ocean-atmosphere system to a sudden change in the Thermohaline Circulation. Geophys Res Lett 29 (15): doi:10.1029/2002GL015229

Dong BW, Sutton RT (2005) Mechanism of interdecadal thermohaline circulation variability in a coupled ocean-atmosphere GCM. J. Climate 18: 1117–1135. doi: 10.1175/JCLI3328.1

Dong, BW, Sutton RT, Scaife AA (2006) Multidecadal modulation of El Niño Southern Oscillation (ENSO) variance by Atlantic Ocean sea surface temperatures. Geophys Res Lett 3: L08705. doi:10.1029/2006GL025766

Dong BW, Sutton RT (2007) Enhancement of ENSO Variability by a Weakened Atlantic Thermohaline Circulation in a Coupled GCM. J. Clim 20: 4920-4939. doi: 10.1175/JCLI4282.1

Dong BW, Sutton RT, Scaife AA (2006) Multidecadal modulation of El Nino Southern Oscillation (ENSO) variance by Atlantic Ocean sea surface temperatures. Geophys Res Lett 3**:** L08705. doi:10.1029/2006GL025766

778 Dong S, Kelly K (2004) Heat Budget in the Gulf Stream Region: The Importance of Heat
779 Storage and Advection. J Phys Ocean 34: 1214-1231
780 Eden C, Jung T (2001) North Atlantic Interdecadal Variability: Oceanic Response to the
781 North Atlantic Oscillation. J Clim 14: 676-691
782 Elsner JB, Tsonis AA (1996) Singular Spectrum Analysis: A New Tool in Time Series
783 Analysis. Springer, 177 pp.
784 Enfield DB, Mestas-Nuñez AM (1999) Multiscale Variabilities in Global Sea Surface
785 Temperatures and Their Relationships with Tropospheric Climate Patterns. J.
786 Clim 12: 2719-2733
787 Enfield DB, Mestas-Nuñez AM, Trimble PJ (2001) The Atlantic Multidecadal oscillation
788 and its relation to rainfall and river flows in the continental U. S. Geophys Res
789 Lett 28: 277-280
790 Federov A, Philander SG (2000) Is El Niño Changing? Science 288**:** 1997-2002. doi:
791 10.1126/science.288.5473.1997
792 Folland CK, Palmer TN, Parker DE (1986) Sahel rainfall and worldwide sea temperature
793 1901-1985. Nature320: 602-607
794 Frankignoul C, Sennechael N, Kwon Y, Alexander M (2011) Influence of the Meridional
795 Shifts of the Kuroshio and the Oyashio Extensions on the Atmospheric
796 Circulation. J.Clim 24:762-777, doi 10.1175/2010 JCLI 3731.1
797 Georgieva K, Kirov B, Tonev P, Guineva V, Atanasov D (2007) Long-term variations in
798 the correlation between NAO and solar activity: the importance of north-south
799 solar activity asymmetry for atmospheric circulation. Adv in Space Res 40: 1152-
800 1166. doi: 10.1016/j.asr.2007.02.091

801 Getzlaff J, Böning CW, Eden C, Biastock A (2005) Signal propagation related to the North
802 Atlantic overturning. Geophys Res Lett 32: doi:10.1029/2004GL021002
803 Ghil M, Vautard R (1991) Interdecadal oscillations and the warming trend in global
804 temperature time series. Nature 305: 324–327
805 Ghil M, Allen MR, Dettinger MD, Ide K, Kondrashov D, Mann ME, Robertson AW,
806 Saunders A, Tian Y, Varadi F, Yiou P (2002) Advanced spectral methods for
807 climatic time series. Rev Geophys **40**(1): 3.1–3.41. doi:10.1029/2000GR000092.
808 Girs AA (1971) Girs AA (1971) Multiyear oscillations of atmospheric circulation and
809 long-term meteorological forecasts. L. Gidrometeroizdat 480 p. (in Russian)
810 Girs AA (1974) Macrocirculation method for long-term meteorological prognosis.
811 Hydrometizdat Publ, Leningrad, 480p. (in Russian)
812 Girs AA, Kondraovich KV (1978) Methods of Long Term Weather Forecasts.
813 Gidrometeroizdat, Leningrad (in Russian).
814 Gray ST, Graumlich LJ, Betancourt JL, Pederson GT (2004) A tree-ring based
815 reconstruction of the Atlantic Multidecadal Oscillation since 1567 A.D. Geophys
816 Res Lett 31. L12205: doi:10.1029/2004GL019932
817 Grosfeld K, Lohmann G, Rimbu N, Fraedrich K, Lunkeit F (2007) Atmospheric
818 multidecadal variations in the North Atlantic realm: proxy data, observations, and
819 atmospheric circulation model studies. Clim of the Past 3: www.clim-
820 past.net/3/39/2007 :39-50
821 Grosfeld K, Lohmann G, Rimbu N (2008) The impact of Atlantic and Pacific Ocean sea
822 surface temperature anomalies on the North Atlantic multidecadal variability.
823 Tellus A: doi: 10.1111/j.1600-0870.2008.00304.x
824 Hakkinen S (1999) A Simulation of Thermohaline Effects of a Great Salinity Anomaly. J

825 Clim12: 1781-1795
826 Hansen DV, Bedzek HF (1996) On the nature of decadal anomalies in North Atlantic
827 SST. JGR 101: 8749-8758
828 Hasegawa T, Yasuda T, Hanawa K (2007) Multidecadal Variability of the Upper Ocean
829 Heat Content Anomaly Field in the North Pacific and its Relationship to the
830 Aleutian Low ans the Kuroshio Transport. Papers in Meteorology and Geophysics
831 58: 155-166: doi: 10.2467/mripapers.58.155
832 Hasselmann K (1976) Stochastic climate models.Pt.1. Tellus 28:473-485
833 Hilmer M, Jung T (2000) Evidence for a recent change in the link between the North
834 Atlantic Oscillations and Arctic sea ice export. Geophys Res Lett 27(7): 989-992.
835 doi: 10.1029/1999GL010944
836 Hurrell JW (1995) Decadal Trends in the North Atlantic Oscillation: Regional
837 Temperatures and Precipitation. Science 269: 676-679
838 Hurrell JW (2003) The North Atlantic Oscillation: Climatic significance and
839 environmental effect. EOS 84(8): 73
840 Jones PD, Moberg A (2003) Hemispheric and large-scale surface air temperature
841 variations: an extensive revision and an update to 2001. J Clim 16: 206-223.
842 doi:10.1175/1520-0442(2003)
843 Jungclaus JH, Haak H, Latif M, Mikolajewicz U (2005) Arctic-North Atlantic
844 Interactions and Multidecadal Variability of the Meridional Overturning
845 Circulation. J Clim 18: 4013-4031. doi: 10.1175/JCLI3462.1
846 Kaplan A, Cane M, Kushnir Y, Clement A, Blumenthal M, Rajagopalan B (1998)
847 Analyses of global sea surface temperature 1856–1991. J Geophys Res 103: 18,

567–18, 589.

Keenlyside N.S., Latif M, Jungclaus J, Kornblueh L, Roeckner E (2008) Advancing decadal-scale climate prediction in the North Atlantic sector. Nature 453: 84-88. doi:10.1038/nature06921.

Kelly K, Dong S (2004) The Relationship of Western Boundary Current Heat Transport and Storage to Midlatitude Ocean-Atmosphere Interaction. Ocean-Atmosphere Interaction and Climate Variability, Edited by Chunzai Wang, Shang-Ping Xie, and James A. Carton, AGU Monograph

Kelly K, Small RJ, Samelson RM, Qiu B, Joyce TM, Kwon Y-O, Cronin MF (2010) Western Boundary Currents and Frontal Air-Sea Interaction: Gulf Stream and Kuroshio Extension. J Climate 23: 5644-5667. DOI: 10.1175/2010JLCI3346.1

Kerr RA (2000) A North Atlantic climate pacemaker for the centuries. Science 288: 1984-1986. doi: 10.1126/science.288.5473.1984

Kirov B, Georgieva K (2002) Long-term variations and interrelations of ENSO, NAO, and solar activity. Physics and Chemistry of the Earth 27: 441-448

Klyashtorin LB Lyubushin AA (2007) Cyclic Climate Changes and Fish Productivity. Moscow, VNIRO Publishing, Editor for English version: Dr. Gary D. Sharp, Center for Climate/Ocean Resources Study, Salinas, CA. USA: 223pp

Knight JR, Allan RJ, Folland CK, Vellinga M, Mann ME (2005) A signature of persistent natural thermohaline circulation cycles in observed climate Geophy Res Lett 32: L20708. doi: 10.1029/2005GRL024233

Knight JR, Folland CK, Scaife AA (2006) Climate impacts of the Atlantic Multidecadal Oscillation. Geophys Res Lett 33: L17706. doi:10.1029/2006GL026242

871 Kondrashov D, Ghil M (2006) Spatio-temporal filling of missing points in geophysical
872 data sets. Nonl Proc Geophys 13: 151–159
873 Kravtsov S (2010) An empirical model of decadal ENSO variability. J Climate, submitted
874 Kravtsov S, Dewar WK, Ghil M, McWilliams JC, Berloff P (2008) A mechanistic model
875 of mid-latitude decadal climate variability. Physica D 237: 584–599.
876 doi:10.1016/j.physd.2007.09.025
877 Kravtsov S, Kondrashov D, Ghil M (2005) Multi-level regression modeling of nonlinear
878 processes: Derivation and applications to climatic variability. J Climate 18: 4404–
879 4424. doi: 10.1175/JCLI3544.1
880 Kug J-S, Jin F-F (2009) Left-hand rule for synoptic eddy feedback on low-frequency
881 flow. Geophys Res Lett 36: L05709. doi: 10.1029/2008GL036435
882 Kushnir Y (1994) Interdecadal Variations in North Atlantic Sea Surface Temperature and
883 Associated Atmospheric Conditions. J Climate 7(1): 141-157
884 Kushnir Y, Held I (1996) Equilibrium atmospheric response to North Atlantic SST
885 anomalies. J Climate 9: 1208-1220
886 Kushnir Y, Robinson WA, Blade I, Hall NMJ, Peng S, Sutton R (2002) Atmospheric
887 GCM response to extratropical SST anomalies: Synthesis and evaluation. J.
888 Climate 15: 2233–2256
889 Kwon Y, Alexander MA, Bond NA, Frankignoul C, Nakamura H, Qiu B, Thompson L
890 (2010) Role of the Gulf Stream and Kuroshio-Oyashio Systems in Large-Scale
891 Atmosphere-Ocean Interaction: A Review. J Climate special collection: DOI:
892 10.1175/2010JCLI3343.1
893 Latif M, Barnett TP (1994) Causes of Decadal Climate Variability over the North Pacific

894 and North America. Science 266: 634-637
895 Latif M, Barnett TP (1996) Decadal Climate Variability over the North Pacific and North
896 America: Dynamics and Predictability. J Climate 9: 2407-2423
897 Latif M, Arpe K, Roeckner E (2000) Oceanic control of decadal North Atlantic sea level
898 pressure variability in winter. Geophys Res Lett 27: 727-730. doi:
899 10.1029/1999GL002370
900 Latif M, Roeckner E. , Botzet M, Esch M, Haak H, Hagemann S, Jungclaus J, Legutke S,
901 Marsland S, Mikolajewicz U, Mitchell J (2004) Reconstructing, Monitoring, and
902 Predicting Decadal-Scale Changes in the North Atlantic Thermohaline Circulation
903 with Sea Surface Temperature . J Climate 17: 1605-1614. doi: 10.1175/1520-
904 0442(2004)
905 Latif M, Böning C, Willebrand J, Biastoch A, Dengg J, Keenlyside N, Schweckendiek U,
906 Madec G (2006) Is the thermohaline circulation changing? J Climate 19 (18):
907 4631-4637. doi: 10.1175/JCLI3876.1
908 Lau N-C (1988) Variability of the observed midlatitude storm tracks in relation to low-
909 frequency changes in the circulation pattern. J Atmos Sci 45: 2718-2743
910 Lau N-C, Nath MJ (1994) A modeling study of the relative roles of tropical and
911 extratropical SST anomalies in the variability of the global atmosphere-ocean
912 system. J Climate 7: 1184-1207
913 Mann ME, Park J (1994) Global-scale modes of surface temperature variability on
914 interannual to century timescales. J Geophys Res 99: 25819–25833
915 Mann ME, Park J, Bradley RS (1995) Global interdecadal and century-scale oscillations
916 during the past five centuries. Nature 378: 266-270

917 Mann ME, Park J (1996) Joint Spatiotemporal Modes of Surface Temperature and Sea
918 Level Pressure Variability in the Northern Hemisphere during the Last Century. J.
919 Climate 9: 2137-2162
920 Mann ME, Bradley RS, Hughes MK (1998) Global-scale temperature patterns and
921 climate forcing over the past six centuries. Nature 392: 779-787
922 Mantua NJ, Hare SR, Zhang Y, Wallace JM, Francis RC (1997) A Pacific interdecadal
923 climate oscillation with impacts on salmon production. Bull Amer Meteor Soc 78:
924 1069-1079
925 Marshall J, Johnson H, Goodman J (2001a) A study of the interaction of the North
926 Atlantic Oscillation with ocean circulation. J Climate 14: 1399–1421
927 Marshall J, Kushnir Y, Battisti D, Chang P, Czaja A, Dickson R, Hurrell J, McCartney
928 M, Saravanan R, Visbeck M (2001b) North Atlantic climate variability:
929 phenomena, impacts and mechanisms. Internat J Climatology 21: 1863–1898. doi:
930 10.1002/joc.693
931 McCartney M (1997) Climate change: Is the ocean at the helm? Nature 388: 521-522
932 Meehl GA, Covey C, Delworth T, Latif M, McAveney B, Mitchell JFB, Stouffer RJ,
933 Taylor KE (2007) The WCRP CMIP3 Multimodel Dataset: A new era in climate
934 change research. Bull Amer Meteo Soc 88(9): 1383-1394. doi: 10.1175/BAMS-
935 88-9-1383
936 Mehta VM, Suarez MJ, Manganello JV, Delworth TL (2000) Oceanic influence on the
937 North Atlantic oscillation and associated Northern Hemisphere climate variations:
938 1959-1993. Geophys Res Lett 27(1): 121-124. doi: 10.1029/1999GL002381

939 Metzger EJ, Hurlburt HE (2001) The importance of high horizontal resolution and
940 accurate coastline geometry in modeling South China Sea Inflow. Geophys Res
941 Lett 28(6): 1059-1062. doi: 10.1029/2000GL012396
942 Miller AJ, Chai Fei, Chiba S, Moisan JR, Neilson DJ Decadal-Scale Climat and
943 Ecosystem Interactions in the North Pacific Ocean (2004). J of Oceanog (60)
944 163:188.
945 Minobe S (1997) A 50-70-year climatic oscillation over the North Pacific and North
946 America. Geophys Res Lett 24: 683-686
947 Minobe S (1999) Resonance in bidecadal and pentadecadal climate oscillations over the
948 North Pacific: role in climatic regime shifts. Geophys Res Lett 26: 855-858
949 Minobe S, Kuwano-Yoshida A, Komori N, Xie S-P, Small RJ (2008) Influence of the
950 Gulf Stream on the troposphere. Nature 452: 206-209. doi: 10.1038/nature06690
951 Moron V, Vautard R, Ghil M (1998) Trends, interdecadal and interannual oscillations in
952 global sea-surface temperatures. Climate Dyn 14: 545–569.
953 Msadek R, Dixon KW, Delworth TL, Hurlin W (2010a) Assessing the predictability of
954 the Atlantic meridional overturning circulation and associated fingerprints.
955 Geophys Res Lett 37: L19608. doi: 10.1029/2010GL044517
956 Msadek R, Frankignoul C, Li LZX (2010b) Mechanisms of the atmospheric response to
957 North Atlantic multidecadal variability: a model study. Climate Dyn online: DOI
958 10.1007/s00382-010-0958-0
959 Nakamura H, Sampe T, Tanimoto Y, Shimpo A (2004) Observed Associations Among
960 Storm Tracks, Jet Streams, and Midlatitude Ocean Fronts. from AGU

961 Monograph: The Earth's Climate: The Ocean-Atmosphere Interaction
962 Geophysical Monograph 147: 329-346. doi: 10.1029/147GM18
963 North GR, Bell TL, Cahalan RF, Moeng FJ (1982) Sampling errors in the estimation of
964 empirical orthogonal functions. Mon Wea Rev 110, 669–706
965 Overland JE, Adams JM, Bond NA (1999) Decadal Variability of the Aleutian Low and
966 Its Relation to High-Latitude Circulation. J Climate12: 1542-1548
967 Palmer TN, Sun Z (1985) A modeling and observational study of the relationship
968 between sea surface temperature in the northwest Atlantic and the atmospheric
969 general circulation. QJR Meteorol Soc 111: 947-975
970 Pan L-L (2007) Synoptic eddy feedback and air-sea interaction in the North Atlantic
971 region. Clim Dyn 29: 647-659. DOI: 10.1007/s00382-007-0256-7
972 Peng S, Robinson WA, Hoerling MP (1997) The modeled atmospheric response to
973 midlatitude SST anomalies and its dependence on background circulation states. J
974 Climate 10: 971-987
975 Peng S, Whitaker JS (1999) Mechanisms Determining the Atmospheric Response to
976 Midlatitude SST Anomalies. J Climate 12: 1393-1408
977 Peng S, Robinson WA (2001) Relationships between atmospheric internal variability and
978 the response to an extratropical SST anomaly. J Climate 14: 2943-2959.
979 doi:10.1175/1520-0442(2001)
980 Peng S, Robinson WA, Li S (2002) North Atlantic SST forcing of the NAO and
981 relationships with intrinsic hemispheric variability. Geophys Res Lett 29: 1276.
982 doi: 10.1029/2001GL014043
983 Penland, C (1989) Random forcing and forecasting using principal oscillation pattern

analysis. Mon Wea Rev 117: 2165–2185

Penland, C (1996) A stochastic model of Indo-Pacific sea-surface temperature anomalies. Physica D 98: 534–558

Penland C, Ghil M (1993) Forecasting Northern Hemisphere 700-mb geopotential height anomalies using empirical normal modes. Mon Wea Rev 121: 2355–2372

Pohlmann H, Sienz F, Latif M (2006) Influence of the Multidecadal Atlantic Meridional Overturning Circulation Variability on European Climate. J Climate (special section) 19: 6062-6067. doi: 10.1175/JCLI3941.1

Polonsky AB (1997) Variability in the NW Black Sea associated with the large-scale atmospheric processes. Meteor and Hydrol 3: 59-70 (in Russian)

Polonsky AB (2001) The role of the ocean in the recent climate changes. Marine Hydrophys. Journal 6: 32-58 (in Russian).

Polonsky AB, Basharin DV, Voskresenskaya EN, Worley SJ, Yurovsky AV (2004) Relationship between the North Atlantic Oscillation, Euro-Asian climate anomalies and Pacific variability. Marine Meteorology. Pacific Oceanography 2(1-2): 52-66

Polyakov IV, Alexeev VA, Bhatt US, Polyakova EI, Zhang X (2009) North Atlantic warming: patterns of long-term trend and multidecadal variability. Clim Dyn (Springerlink.com). DOI: 10.1007/s00382-008-0522-3

Preisendorfer RW (1988) Principal component analysis in Meteorology and Oceanography. Elsevier, Amsterdam, 425pp

Press, WH, Teukolsky SA, Vetterling WT, Flannery, BP (1994) Numerical Recipes. 2nd edition, Cambridge University Press, 994pp

1007 Rayner NA, Brohan P, Parker DE, Folland CK, Kennedy J, Vanicek M, Ansell T, Tett
1008 SFB (2006) Improved analyses of changes and uncertainties in sea-surface
1009 temperature measured in situ since the mid-nineteenth century. J Climate 19: 446-
1010 469. doi: 10.1175/JCLI3637.1
1011 Robertson AW, Mechoso CR, Kim Y-J (2000) The influence of Atlantic sea surface
1012 temperature anomalies on the North Atlantic Oscillation. J Climate 13: 122-138.
1013 doi: 10.1175/1520-0442(2000)
1014 Rodwell MJ, Rowell DP, Folland CK (1999) Oceanic forcing of the wintertime North
1015 Atlantic Oscillation and European climate. Nature 398: 320-323
1016 Roe G (2009) Feedbacks, Timescales, and Seeing Red. Annu Rev Earth Planet Sci 37:
1017 5.1-5.23. doi: 10.1146/annurev.earth.061008.134734
1018 Rogers JC (1981) The North Pacific Oscillation. Int J Climatol 1: 39-57
1019 Rotstayn L.D, Lohman U (2002) Tropical rainfall trends and the indirect aerosols effect. J
1020 Climate 15: 2103-2116
1021 Schlesinger ME, Ramankutty N (1994) An oscillation in the global climate system of
1022 period 65-70 years. Nature 367: 723-726
1023 Schneider T (2001) Analysis of incomplete climate data: estimation of mean values and
1024 covariance matrices and imputation of missing values. J Climate 14: 853–871.
1025 doi: 10.1175/1520-0442(2001)
1026 Schneider N, Miller AJ, Pierce DW (2002) Anatomy of North Pacific decadal
1027 variability. J Climate 15: 586–605. doi: 10.1175/1520-0442(2002)
1028 Shabalova MV, Weber SL (1999) Patterns of temperature variability on multidecadal to
1029 centennial timescales. J Geophys Res 104: 31,023-31,041

1030 Shaffrey L, Sutton R (2006) Bjerknes Compensation and the Decadal Variability of the
1031 Energy Transports in a Coupled Climate Model. J Clim19: 1167-1181. doi:
1032 10.1175/JCLI3652.1
1033 Shindell DT, Schmidt GA, Miller RL, Rind D (2001) Northern Hemisphere winter
1034 climate response to greenhouse gas, ozone, solar, and volcanic forcing. J.
1035 Geophys Res 106: 7193-7210. doi:10.1029/2000JD900547
1036 Stocker TF, Mysak LA (1992) Climatic fluctuations on the century time scale: a review
1037 of high-resolution proxy data and possible mechanisms. Clim Change 20: 227-
1038 250
1039 Stommel H (1961) Thermohaline convection with two stable regimes of flow. Tellus 13:
1040 224–230
1041 Stott PA, Tett SFB, Jones GS, Allen MR, Mitchell JFB, Jenkins GJ (2000) External
1042 Control of 20th Century Temperature by Natural and Anthropogenic Forcings.
1043 Science 290: 2133-2137. DOI: 10.1126/science.290.5499.2133
1044 Sugimoto S, Hanawa K (2009) Decadal and Interdecadal Variations of the Aleutian Low
1045 Activity and Their Relation to Upper Oceanic Variations over the North Pacific.
1046 Journal of the Meteorological Society of Japan 87 (4): 601-614.
1047 DOI:10.2151/jmsj.87.601
1048 Sutton RT, Allen MR (1997) Decadal predictability of North Atlantic sea surface
1049 temperature and climate. Nature 388: 563-567
1050 Sutton RT, Hodson DLR (2003) Influence of the Ocean on North Atlantic Climate
1051 Variability 1871-1999. J Climate 16: 3296-3313. doi: 10.1175/1520-0442(2003)

1052 Sutton RT, Hodson DLR, Mathieu P (2003) The Role of the Atlantic Ocean in Climate
1053 Forecasting, Proceedings of the ECMWF Workshop on the Role of the Upper
1054 Ocean in Medium and Extend Range Forecasting, ECMWF, Reading, UK
1055 Sutton RT, Hodson DLR (2005) Atlantic Ocean forcing of North American and European
1056 summer climate. Science 309: 115-118. doi: 10.1126/science.1109496
1057 Sutton RT, Hodson DLR (2007) Climate response to basin-scale warming and cooling of
1058 the North Atlantic Ocean. J Climate 20: 891-907. doi: 10.1175/JCLI4038.1
1059 Swanson K, Tsonis AA (2009) Has the climate recently shifted? Geophys Res Lett 36.
1060 doi:10.1029/2008GL037022
1061 Taylor KE, Stouffer RJ, Meehl GA (2008) A Summary of the CMIP5 Experiment
1062 Design.http://www.pcmdi.llnl.gov/ipcc/model_documentation/ipcc_model_docu
1063 mentation.php
1064 Timlin MS, Alexander MA (2002) On the Reemergence of North Atlantic SST
1065 Anomalies. J Climate 15: 2707-2712. doi:10.1175/1520-0442(2002)
1066 Timmermann A, Latif M, Voss R, Grotzner A (1998) Northern Hemispheric interdecadal
1067 variability: a coupled air-sea mode. J Climate 11: 1906-1931
1068 Timmermann A, Okumura Y, An SI, Clement A, Dong B, Guilyardi E, Hu A, Jungclaus
1069 JH, Renold M, Stocker TF, Stouffer RJ, Sutton R, Xie SP, Yin J (2007) The
1070 influence of a weakening of Atlantic meridional overturning circulation on
1071 ENSO. J Climate 20: 4899–4919. doi:10.1175/JCLI4283.1
1072 Tsonis AA, Swanson K, Kravtsov S (2007) A new dynamical mechanism for major
1073 climate shifts. Geophys Res Lett 34: L13705. doi:10.1029/2007GL030288
1074 Van der Swaluw E, Drijfhout SS, Hazeleger W (2007) Bjerknes Compensation at High

1075 Northern Latitudes: The Ocean Forcing the Atmosphere. J Climate 20: 6023-
1076 6032. doi: 10.11752007JCLI1562.1
1077 Vangenheim GYa (1940) The long-term temperature and ice break-up forecasting. Proc
1078 State Hydrological Institute Iss. 10: 207-236 (in Russian)
1079 Vautard R, Ghil M (1989) Singular spectrum analysis in nonlinear dynamics, with
1080 applications to paleoclimatic time series. Physica D 35: 395–424
1081 Vautard R, Yiou P, Ghil M (1992) Singular Spectrum Analysis: A toolkit for short, noisy
1082 and chaotic series. Physica D 58: 95 - 126
1083 Vellinga M, Wood RA (2002) Global climatic impacts of a collapse of the Atlantic
1084 thermohaline circulation. Climatic Change 54: 251-267. doi:
1085 10.1023/A:1016168827653.
1086 Vellinga M, Wu P (2004) Low-latitude freshwater influence on centennial variability of
1087 the Atlantic thermohaline circulation. J Climate 17: 4498-4511.
1088 doi:10.1175/3219.1
1089 Vimont DJ, Battisti DS, Hirst AC (2001) Footprinting: A seasonal connection between
1090 the Tropics and mid-latitudes. Geophys Res Lett 28: 3923:3926.
1091 Vimont DJ, Battisti DS, Hirst AC (2003a) The seasonal Footprinting mechanism in the
1092 CSIRO general circulation models. J Climate 16: 2653-2667. doi:10.1175/1520-
1093 0442(2003)
1094 Vimont DJ, Wallace JM, Battisti DS (2003b) The Seasonal Footprinting Mechanism in
1095 the Pacific: Implications for ENSO. J Clim 16: 2668-2675.
1096 Vimont DJ, Kossin JP (2007) The Atlantic Meridional Mode and hurricane activity.
1097 Geophy Res Lett 34: L07709. doi:10.1029/2007/GL029683

1098 Walker GT, Bliss EW (1932) World weather. Mem R Met Soc 4: 53-84
1099 Wallace JM, Gutzler DS (1981) Teleconnections in the geopotential height field during
1100 the Northern Hemisphere winter. Mon Wea Rev 109: 784-812.
1101 Wang L, Chen W, Huang R (2007) Changes in the Variability of North Pacific
1102 Oscillation around 1975/1976 and its relationship with East Asian winter climate.
1103 J Geophys Res 112: D11110. doi: 10.1029/2006JD008054
1104 Willis JK, Roemmich D, Cornuelle B (2004) Interannual variability in upper ocean heat
1105 content, temperature, and thermosteric expansion on global scales. J Geophys Res
1106 109: C12036. doi: 10.1029/2003C002260
1107 Wu P, Gordon C (2002) Oceanic Influence on North Atlantic Climate Variability. J
1108 Climate 15: 1911-1925. doi: 10.1175/1520-0442(2002)
1109 Wu LP, Rodwell M (2004) Gulf Stream forcing of the winter North Atlantic oscillation.
1110 Atm Sc Lett 5: 57-64. doi: 10.1016/j.atmoscilet.2003.12.002
1111 Xie SP (2004) Satellite observations of cool ocean-atmosphere interaction. Bull Am
1112 Meteorol Soc 85: 195-208. doi: 10.1175/BAMS-85-2-195
1113 Xie SP, Carton J (2004) Tropical Atlantic Variability: Patterns, Mechansims, and
1114 Impacts. Earth Climate: The Ocean-Atmosphere Interaction. C. Wang, S.P. Xie,
1115 and J. A. Carton (eds.), Geophys Monograph. AGU. Washington, D. C., pp 121-
1116 142. doi: 10.1029/147GM07
1117 Yualeva EN, Schneider N, Pierce DW, Barnett TP (2001) Modeling of North Pacific
1118 climate variability forced by ocean heat flux anomalies. J Climate 14: 4027-4046.
1119 doi: 10.1175/1520-0442(2001)
1120 Zhang YJ, Wallace M, Iwasaka N (1996) Is Climate Variability over the North Pacific a

Linear Response to ENSO? J Climate 9: 1468-1478

Zhang R, Delworth TL (2005) Simulated tropical response to a substantial weakening of the Atlantic thermohaline circulation. J Climate 18: 1853-1860. doi: 10.1175/JCLI3460.1

Zhang R, Delworth TL (**2007**) Impact of Atlantic multidecadal oscillations on India/Sahel rainfall and Atlantic hurricanes. Geophys Res Lett 33: L17712. doi:10.1029/2006GL026267

Zhang R, Delworth TL, Held IM (2007) Can the Atlantic Ocean drive the observed multidecadal variability in Northern Hemisphere mean temperature? Geophys Res Lett 34: L02709. doi:10.1029/2006GL028683

Zhen-Shan L, Xian S (2007) Multi-scale analysis of global temperature changes and trend of a drop in temperature in the next 20 years. Meteor and Atmos Physics: 95: 115-121

Table Captions

Table 1. Observed climate-index network.

Table 2. The stadium-wave lags and their uncertainties (yr) estimated using a bootstrap procedure (see text). The time scale T of the observed stadium-wave cycle is given by the twice-the-sum of first-row values, while its standard uncertainty — by the square root of twice-the-sum of the second row's squared values. These calculations result in the estimate of T=63±5 yr, consistent with the 64-yr scale obtained in the 8-index (and 15-index) M-SSA analyses.

Table 3. Maximum lagged correlations (with corresponding lags) between climate indices computed over the full 100-yr 20th century record, as well as over its second half (1950–1999); the latter correlation values are shown in parentheses. Only the correlations that are statistically significant at 5% *a posteriori* level for *both* of these periods — relative to the null hypothesis of zero correlation at any lag — are shown. Correlations equal or exceeding 0.5 (upon rounding up) are in bold font. The negative lags correspond to the column-member of an index pair leading its corresponding row member*. For example, the maximum lagged correlation between NINO3.4 and PNA is equal to 0.47 (0.54 during the second half of the 20th century), with NINO3.4 leading by 1 yr.

* Note: "column-members" arranged in the leftmost column; "row-members" arranged in the top row.

Figure Captions

Fig. 1. M-SSA spectrum of the network of eight climate indices (see text): (a) Individual variances (%); (b) cumulative variance (% of the total). The M-SSA embedding dimension (window size) M=20. The errorbars in (a) are based on North et al. (1982) criterion, with the number of degrees of freedom set to 40, based on the decorrelation time scale of ~2.5 yr. The +-symbols and dashed lines in panel (a) represent the 95% spread of M-SSA eigenvalues base on 100 simulations of the eight-valued red-noise model (1), which assumes zero true correlations between the members of the eight-index set.

Fig. 2. Normalized reconstructed components (RCs) of the eight-index network. The RC time series shown have been normalized to have a unit variance. The indices are synchronized at, generally, non-zero lags, except for the indices NPO and PDO indices, whose rescaled RCs are virtually identical. Note that the reconstructions of *negative* NHT and AMO indices are displayed.

Fig. 3. (a) Fraction of each index variance (%) accounted for jointly by M-SSA modes 1 and 2, as a function of the low-pass filter time scale (yr). Boxcar low-pass filtering has been applied to each index prior to the M-SSA analysis; the value of 0 corresponds to no prior low-pass filtering (the normalized RCs for this case are shown in Fig. 2), the values 10, 20, and 30 indicate 10-yr, 20-yr, and 30-yr running-mean boxcar filtering, with shorter-filter-size running means and one-sided (or asymmetric) filters used to process ends of the plotted curves. (b) Filtered NAO time series: heavy line — 30-yr running-mean boxcar filtered time series; light line — reconstruction based on M-SSA modes 1 and 2 of the 30-yr

low-pass filtered 8-index set; dashed line — reconstruction based on M-SSA modes 1 and 2 of the raw 8-index set (the same as in Fig. 2). All time series have been normalized to have unit variance.

Fig. 4. Hoffmuller diagram of the "stadium-wave" propagation in the phase space of normalized RCs (for M-SSA modes 1 and 2 combined) of the extended set of 15 multidecadal indices (eight of the indices were described above, while the other seven indices are NPGO, OHC700, OHC300, PNA, WP, PMM, and AMM: see **Figs. 5, 6** and text). For the additional indices, only the ones with substantial fraction of variance within leading pair of RCs (see Fig. 5) are shown. The horizontal cross-section in locations marked by index names shown on the left for the original eight indices, and on the right for the additional indices would represent time series of the corresponding index as plotted in Figs. 2 and 5. The indices are sorted from bottom to top of the figure in the order determined by cross-correlation analysis, while the vertical "distance" between each index equals the lead time of maximum cross-correlation between adjacent indices. Negative indices are also included to show one complete cycle (with the estimated period of 64 yr) of the stadium-wave propagation.

Fig. 5. The M-SSA results based on the analysis of the full 15-index data set. The quantities shown describe the statistics of the seven climatic indices considered in addition to the original 8-index set (see Figs. 2 and 3). (a) Fraction of raw-index variance accounted for jointly by M-SSA modes 1 and 2 (Fig. 3a shows this quantity for the original eight indices). (b) The same as in Fig. 2, but for the

1211 additional seven climate indices [see panel (a) and figure legend for abbreviated
1212 index names].

1213 **Fig. 6**. The network of 15 climate indices: (i) M-SSA modes 1 and 2 RCs (blue); and (ii)
1214 anomaly with respect to the corresponding RC (red). The blue and red lines give
1215 the raw climate index (detrended and normalized to have a unit variance). The
1216 abbreviated index names are given in panel captions.

1217 **Fig. 7**. M-SSA spectrum of the Pacific-centered multi-index set consisting of interdecadal
1218 anomalies (Fig. 6, red lines) of PNA, WP, NINO3.4, NPO, PDO, ALPI indices.
1219 The bottom panel shows raw time series of the NINO3.4 index and its RC based
1220 on M-SSA modes 1 and 2.

1221 **Fig. 8**. The M-SSA results for the Pacific-centered index subset (see Fig. 7). See panel
1222 legend for abbreviated index names. Same conventions as in Fig. 5.

1223 **Fig. 9**. Identification of index sub-networks. For a given year (on the vertical axis), bright
1224 yellow and orange cells indicate that there exists at least one six-index network
1225 that includes the index this cell represents (the indices are arranged along the
1226 horizontal axis), which is characterized by the network connectivity exceeding the
1227 95^{th} percentile of the connectivity for *all possible* 6-index networks and for *all*
1228 *years*; the yellow cells are characterized by the connectivity that exceeds the 99^{th}
1229 percentile. See caption to Fig. 10 and text for the definition of network
1230 connectivity. The results for the subset sizes in the range from 4 to 8 (not shown)
1231 are analogous.

1232 **Fig. 10**. The time series of index connectivity for the sub-networks identified in Fig. 9.
1233 The indices comprising each subset are listed in the caption of each panel. The

measure of connectivity used here is the leading singular value of the lower triangular part of the index cross-correlation matrices computed over the 7-yr sliding window. The horizontal dashed lines indicate 5% a priori and a posteriori confidence levels based on the linear stochastic model that reproduces the *climatological* cross-correlations between the indices.

Fig. 11. Anomalies (with respect to the mean value of 1) of NAO (light black line) and Nino3 (light red line) standard deviations, along with the M-SSA mode's 1–2 RC of AT index (heavy blue line; this line is the same as that in the middle panel of Fig. 7, but multiplied here by a factor of 0.1). The Nino3 standard-deviation anomaly has been scaled by a factor of 0.5 for easier visual analysis. The standard deviations for each index shown were computed over the 31-yr-wide sliding window, with shorter-filter-size running means and one-sided (or asymmetric) filters used to process ends of the plotted curves.

1267 **Table 1.** Observed climate-index network.
1268

Index/Acronym	Reference/Data source	Description/General Information
Aleutian Low Pressure Index **AL or ALPI**	Beamish et al. (1997) http://www.pac.dfo-mpo.gc.ca/sci/sa-mfpd/downloads/indices/alpi.txt	Relative intensity of SLP in N.Pacific (~50°N) in winter (DJFM). Calculated as mean area (km^2) w/ SLP<100.5kPa. Expressed as anomaly relative to the 1950–1997 mean.
Atlantic Multidecadal Oscillation Index **AMO**	Kerr (2000);Enfield et al. (2001); Sutton and Hodson (2003) http://www.esrl.noaa.gov/psd/data/timeseries/AMO/	North Atlantic SSTA averaged across 0–60°N, 75–7.5°W; 1871–2003 Monopolar SSTA pattern N. Atlantic
Atlantic Meridional Mode Index **AMM**	Chiang and Vimont (2004) http://www.cdc.noaa.gov/Timeseries/Monthly/AMM/ www.aos.wisc.edu/~dvimont/Research/MModes/Data/AMM.txt	SST projected onto 10-m wind field 21°S to 32°N; 74°W to 15°E;; SST gradient across Intertropical Convergence Zone (ITCZ) in Atlantic. (proxy for position of Atlantic ITCZ) (Observations available from 1949)
Atmospheric-Mass Transfer Anomalies **AT**	Vangenheim (1940); Girs (1971) http://alexeylyubushin.narod.ru/ lyubushin@yandex.ru	Dominance of air transfer direction 30°–80°N; 45–75°E; Proxy for atmospheric-heat transfer; reflects longitudinal/latitudinal shifts in position of atmospheric centers-of-action, w/ implications for hemispheric communication of climate signal.
North Atlantic Oscillation Index **NAO**	Hurrell (1995) http://www.cgd.ucar.edu/cas/jhurrell/indices.data.html#npanom	Normalized SLP difference Azores and Iceland ~ 1st PC (Principal Component) of SLP in the North Atlantic; re-distribution of atmospheric mass b/n subpolar and subtropical latitudes, reflecting jet-stream variations.
Northern Hemisphere Temperature **NHT**	Jones & Moberg (2003); Rayner et al., (2006) ftp://ftp.cru.uea.ac.uk/data http://www.cru.uea.ac.uk/cru/data/temperature/hadcrut3nh.txt	Average surface land and sea-surface temperatures of Northern Hemisphere 1850–2003 NHT characterizes overall climate variability, with strongest changes occurring at high northern latitudes.
El Niño/ Southern Oscillation region 3.4 **NINO3.4**	Calculated from the HadSST1 http://www.cdc.noaa.gov/gcos_wgsp/Timeseries/Data/nino34.long.data	Average SSTA 5°N–5°S; 170°W –120°W Proxy for ENSO behavior
North Pacific Gyre Oscillation Index **NPGO**	Di Lorenzo et al. (2008) http://www.o3d.org/npgo/data/NPGO.txt http://eros.eas.gatech.edu/npgo/	2-nd PC of SSH in NE Pacific. Measures changes in North Pacific gyre circulation (observations available since 1950)
North Pacific Oscillation Index **NPO**	Rogers (1981); Walker and Bliss (1982); Wang et al. (2007) wanglin@mail.iap.ac.cn cw@post.iap.ac.cn	Meridional dipole in SLP over North Pacific; pressure variations b/n Hawaii and Alaska/Alberta, reflective of meridional re-distribution of atmospheric mass. We used that of Wang et al. 2007: 2nd EOF SLPA 100ºE - 120ºW, 0º-90ºN.

Indices of Ocean-Heat-Content Anomalies **OHCA300** **OHCA700**	Willis et al. (2004) jwillis@pacific.jpl.nasa.gov http://www.nodc.noaa.gov/OC5/DATA_ANALYSIS/basin_data.html	Measured in North Pacific for 0 to 300m & 0 to 700m upper layers May serve as proxies for ocean-dynamic-induced SST variations (since these are presumably not confined to the oceanic mixed layer, while those caused by atmosphere-ocean heat flux are). (Observations available since 1955)
Pacific Decadal Oscillation Index **PDO**	Mantua et al. (1997); Minobe (1997, 1999) ftp://ftp.atmos.washington.edu/mantua/pnw_impacts/INDICES/PDO.latest	Leading PC of SSTA north of 20°N in North Pacific, with century-scale globally averaged SSTA removed; Strongly related to intensity and location of Aleutian Low
Pacific Meridional Mode Index **PMM**	Chiang and Vimont (2004) http://www.cdc.noaa.gov/Timeseries/Monthly/PMM www.aos.wisc.edu/~dvimont/Research/MModes/Data/PMM.txt	Anomalous meridional SST gradient across the Intertropical Convergence Zone (ITCZ) in the Pacific; proxy for Pacific ITCZ position; MCA of SST and 10-m winds 32ºN to 21ºS, 175ºE to 95ºW. (observations available since 1949)
Pacific North American Pattern Index **PNA**	Wallace and Gutzler (1981); Bell and Halpert (1995); Overland et al. (1999) http://www.jisao.washington.edu/data/pna/ http://www.cpc.ncep.noaa.gov/products/precip/CWlink/pna/norm.pna.monthly.b5001.current.ascii	Time series related to combination of standardized 500-hPa geopotential height values (Z) in four centers (Wallace and Gutzler 1981); upper tropospheric pattern associated with PDO; associated with intensity variations and longitudinal shifts of the Aleutian Low and with strength and eastward extent of the East Asian jet. PNA = 0.25 * [Z(20N,160W) - Z(45N,165W) + Z(55N,115W) - Z(30N,85W)]. (Observations available since 1951)
West Pacific Pattern Index **WP**	Wallace and Gutzler (1981) http://www.beringclimate.noaa.gov/data/	Difference in the normalized 500-hPa height anomalies between two points (60°N, 155°E and 30°N, 155°E); upper tropospheric pattern associated with NPO. Involves latitudinal shifts of AL, with resulting influence on oceanic-gyre frontal boundary and western-boundary dynamics – a potential "hotspot" of oceanic-atmospheric coupling (Sugimoto and Hanawa 2009) (Observations available since 1950)

1269
1270
1271
1272
1273
1274
1275
1276
1277

Table 2. The stadium-wave lags and their uncertainties (yr) estimated using a bootstrap procedure (see text). The time scale T of the observed stadium-wave cycle is given by twice-the-sum of the first-row values, while its standard uncertainty — by the square root of twice-the-sum of the second row's squared values. These calculations result in the estimate of T=63±5 yr, consistent with the 64-yr scale obtained in the 8-index (and 15-index) M-SSA analyses.

	–NHT → –AMO	AMO → AT	AT → NAO	NAO → NINO3.4	NINO3.4 → NPO/PDO	NPO/PDO → ALPI	ALPI → NHT
Mean	4.3	6.8	2.4	4.8	2.4	2.9	8.2
STD	0.5	0.4	1.3	1.6	1.1	1.3	1.2
½ 95%	0.5	0.5	2.5	3.0	2.0	2.5	2.0

Table 3. Maximum lagged correlations (with corresponding lags) between climate indices computed over the full 100-yr 20th century record, as well as over its second half (1950–1999); the latter correlation values are shown in parentheses. Only the correlations that are statistically significant at 5% *a posteriori* level for *both* of these periods — relative to the null hypothesis of zero correlation at any lag — are shown. Correlations equal or exceeding 0.5 (upon rounding up) are in bold font. The negative lags correspond to the column-member of an index pair leading its corresponding row member*. For example, the maximum lagged correlation between NINO3.4 and PNA is equal to 0.47 (0.54 during the second half of the 20th century), with NINO3.4 leading by 1 yr.

	NPGO	OHC 7	PNA	WP	AMO	NAO	NINO 3.4	PDO
OHC3		**0.9 (0.9), 0**						
PMM	**–0.54 (–0.52), 0**							
NINO3.4			0.47 **(0.54)**, –1	**0.52** (0.49), –1				
NPO				0.45 (0.46), –1			0.36 (0.48), 0	
PDO			**0.75 (0.76), 0**				0.41 **(0.52)**, 1	
ALPI			**0.77 (0.86), 0**					**0.55 (0.64), 0**
AMM					**0.54 (0.6), 1**	**–0.57 (–0.52), 0**		
NHT			0.42 (0.44), 0		**0.66 (0.74) 0**			

* Note: "column-members" arranged in the leftmost column; "row-members" arranged in the top row.

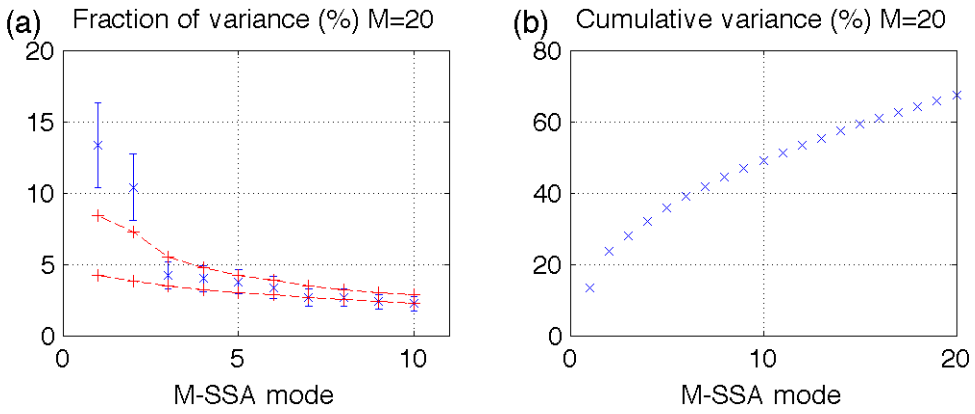

Fig. 1. M-SSA spectrum of the network of eight climate indices (see text): (a) Individual variances (%); (b) cumulative variance (% of the total). The M-SSA embedding dimension (window size) M=20. The errorbars in (a) are based on North et al. (1982) criterion, with the number of degrees of freedom set to 40, based on the decorrelation time scale of ~2.5 yr. The +-symbols and dashed lines in panel (a) represent the 95% spread of M-SSA eigenvalues base on 100 simulations of the eight-valued red-noise model (1), which assumes zero true correlations between the members of the eight-index set.

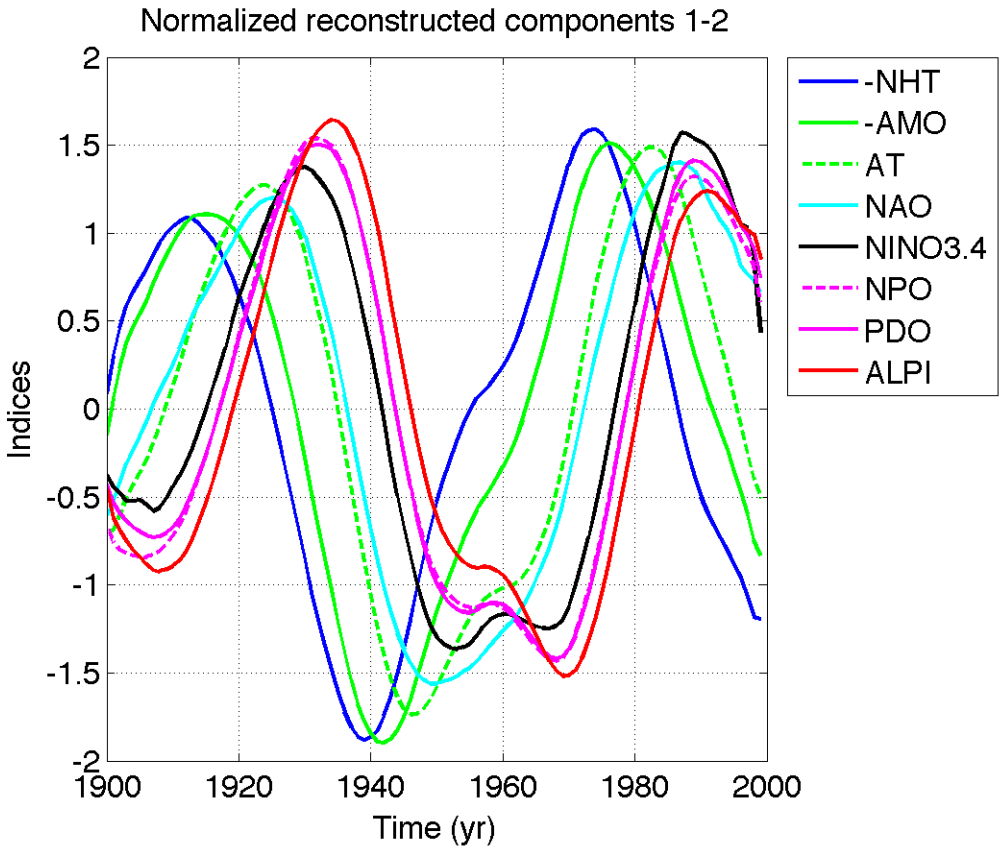

Fig. 2. Normalized reconstructed components (RCs) of the eight-index network. The RC time series shown have been normalized to have a unit variance. The indices are synchronized at, generally, non-zero lags, except for the indices NPO and PDO indices, whose rescaled RCs are virtually identical. Note that the reconstructions of *negative* NHT and AMO indices are displayed.

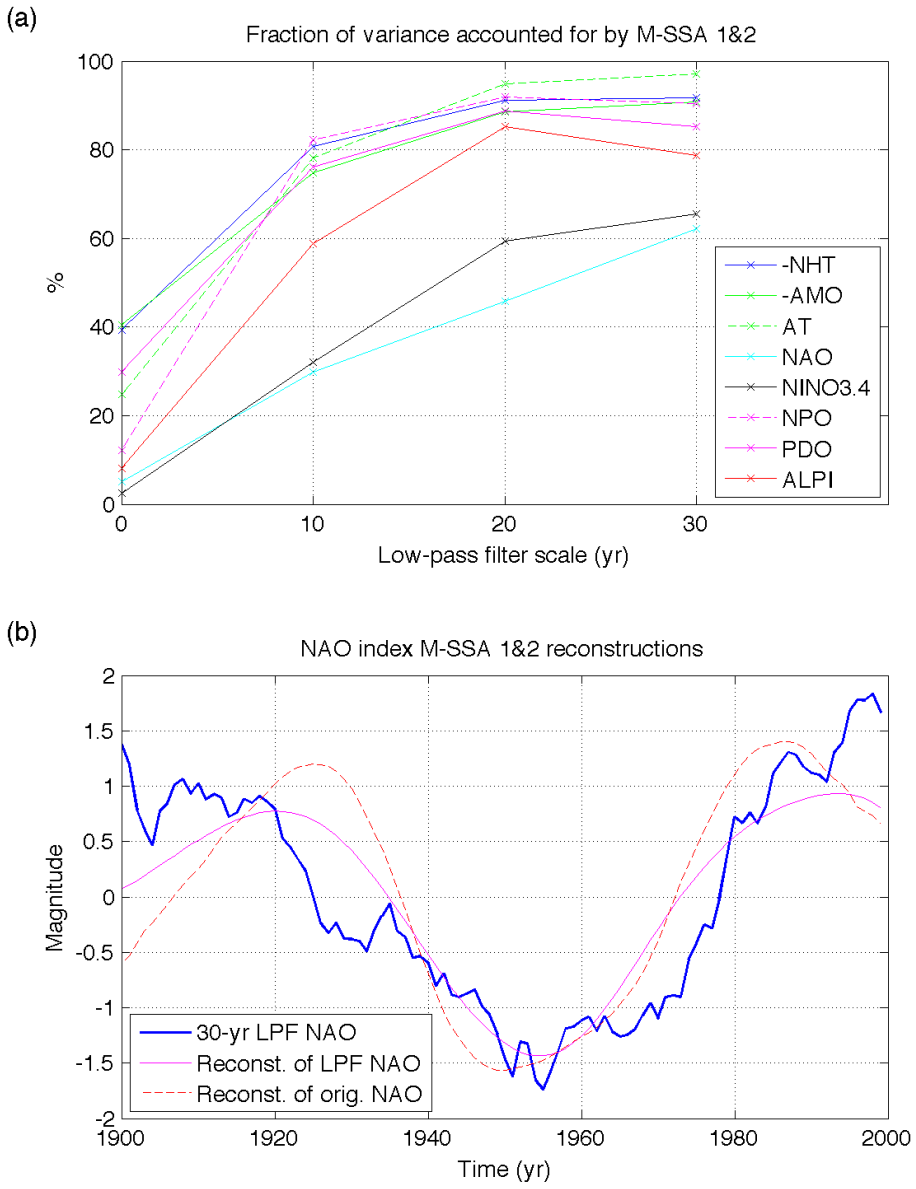

Fig. 3. (a) Fraction of each index variance (%) accounted for jointly by M-SSA modes 1 and 2, as a function of the low-pass filter time scale (yr). Boxcar low-pass filtering has been applied to each index prior to the M-SSA analysis; the value of 0 corresponds to no prior low-pass filtering (the normalized RCs for this case are shown in Fig. 2), the values 10, 20, and 30 indicate 10-yr, 20-yr, and 30-yr running-mean boxcar filtering. (b) Filtered NAO time series: heavy line — 30-yr running-mean boxcar filtered time series; light line — reconstruction based on M-SSA modes 1 and 2 of the 30-yr low-pass filtered 8-index set; dashed line — reconstruction based on M-SSA modes 1 and 2 of the raw 8-index set (the same as in Fig. 2). All time series have been normalized to have unit variance.

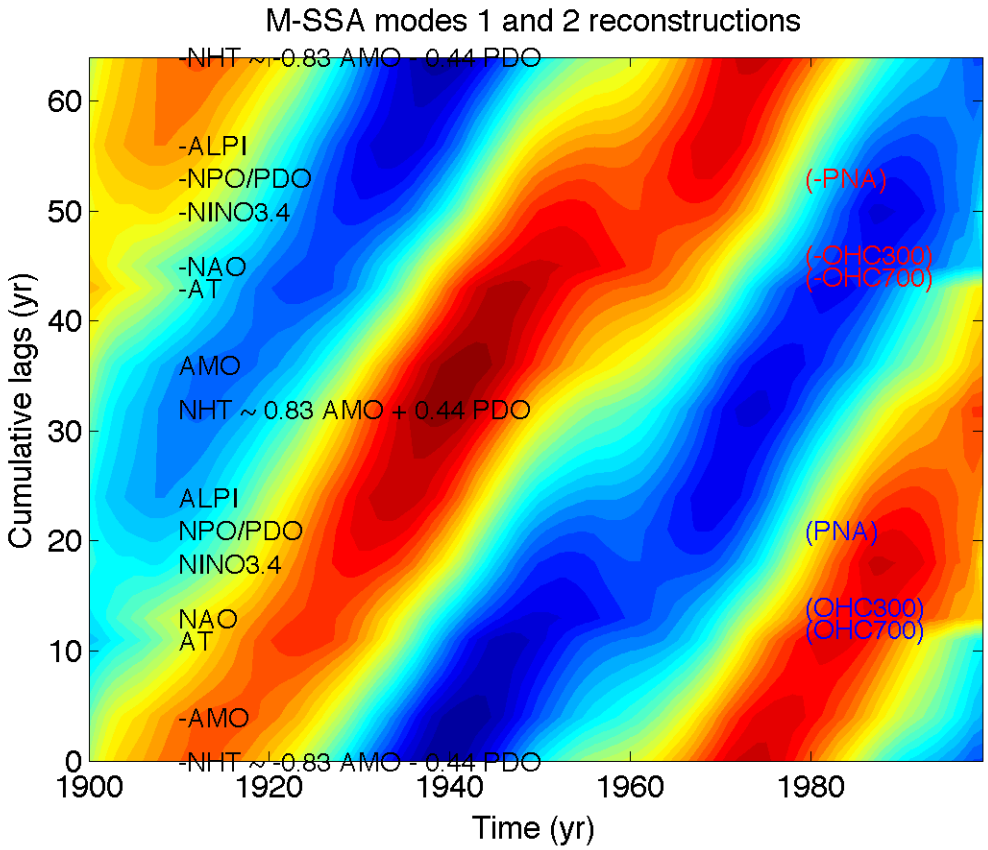

Fig. 4. Hoffmuller diagram of the "stadium-wave" propagation in the phase space of normalized RCs (for M-SSA modes 1 and 2 combined) of the extended set of 15 multidecadal indices (eight of the indices were described above, while the other seven indices are NPGO, OHC700, OHC300, PNA, WP, PMM, and AMM: see **Figs. 5, 6** and text). For the additional indices, only the ones with substantial fraction of variance within leading pair of RCs (see Fig. 5) are shown. The horizontal cross-section in locations marked by index names shown on the left for the original eight indices, and on the right for the additional indices would represent time series of the corresponding index as plotted in Figs. 2 and 5. The indices are sorted from bottom to top of the figure in the order determined by cross-correlation analysis, while the vertical "distance" between each index equals the lead time of maximum cross-correlation between adjacent indices. Negative indices are also included to show one complete cycle (with the estimated period of 64 yr) of the stadium-wave propagation.

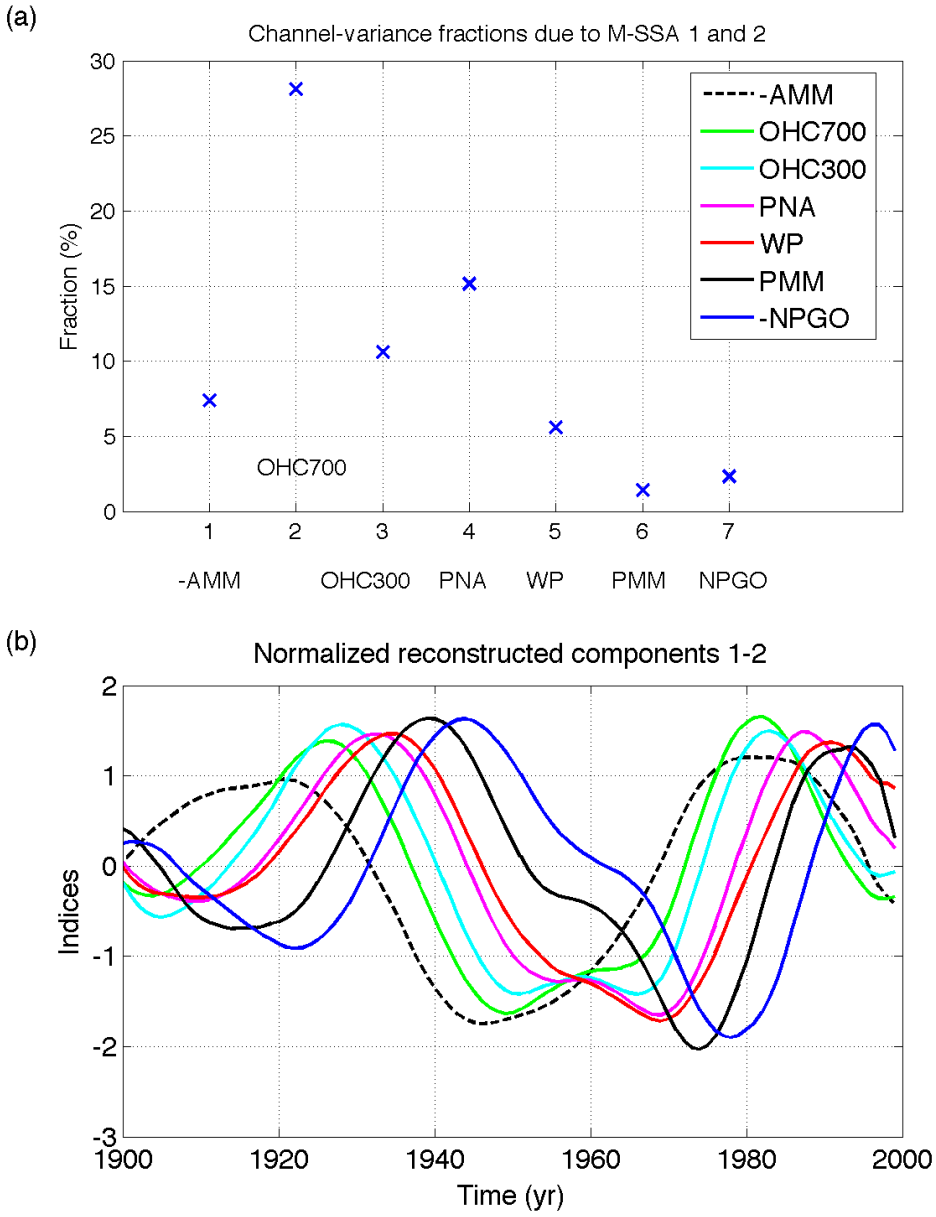

Fig. 5. The M-SSA results based on the analysis of the full 15-index data set. The quantities shown describe the statistics of the seven climatic indices considered in addition to the original 8-index set (see Figs. 2 and 3). (a) Fraction of raw-index variance accounted for jointly by M-SSA modes 1 and 2 (Fig. 3a shows this quantity for the original eight indices). (b) The same as in Fig. 2, but for the additional seven climate indices [see panel (a) and figure legend for abbreviated index names].

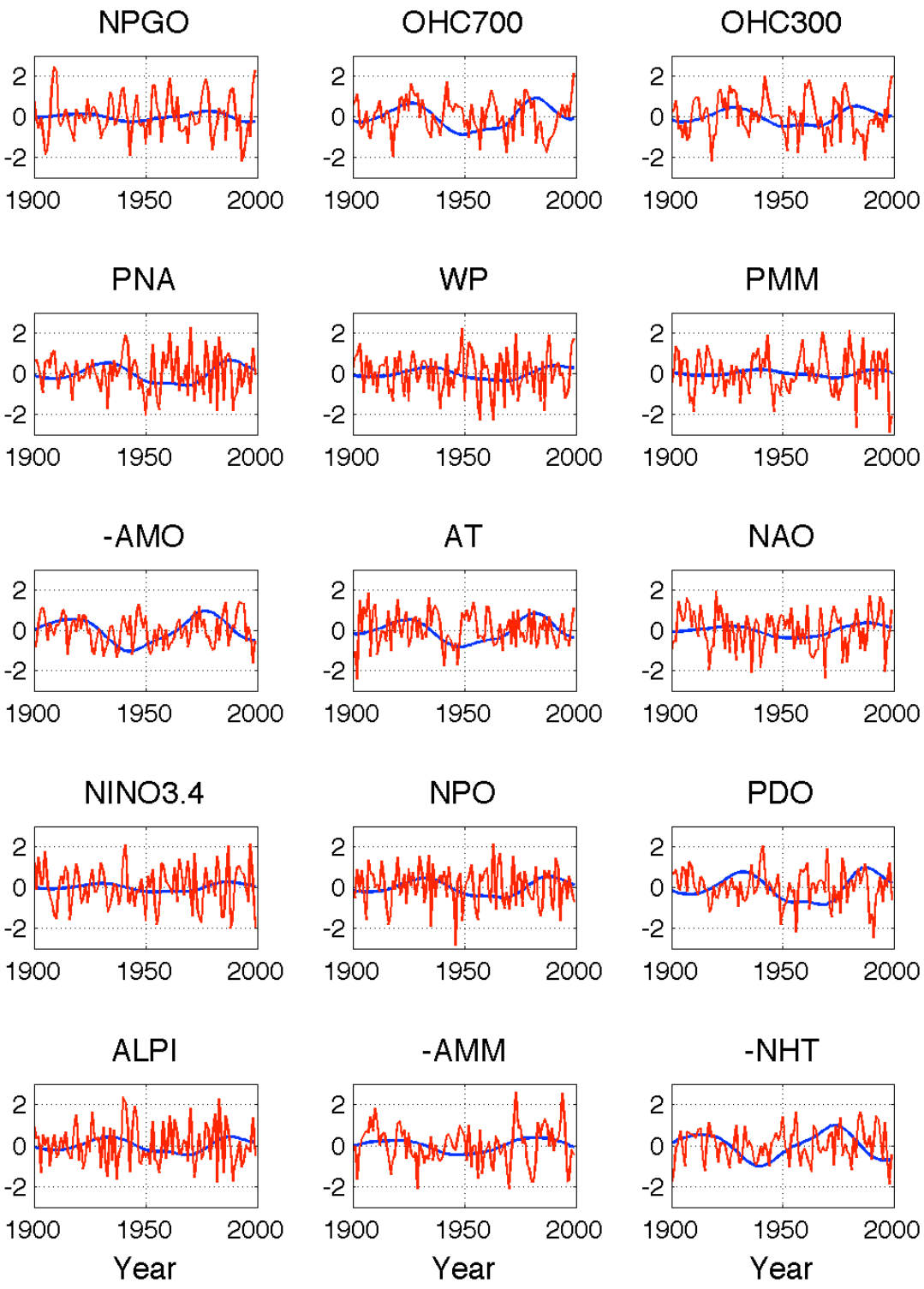

Fig. 6. The network of 15 climate indices: (i) M-SSA modes 1 and 2 RCs (blue); and (ii) anomaly with respect to the corresponding RC (red). The blue and red lines give the raw climate index (detrended and normalized to have a unit variance). The abbreviated index names are given in panel captions.

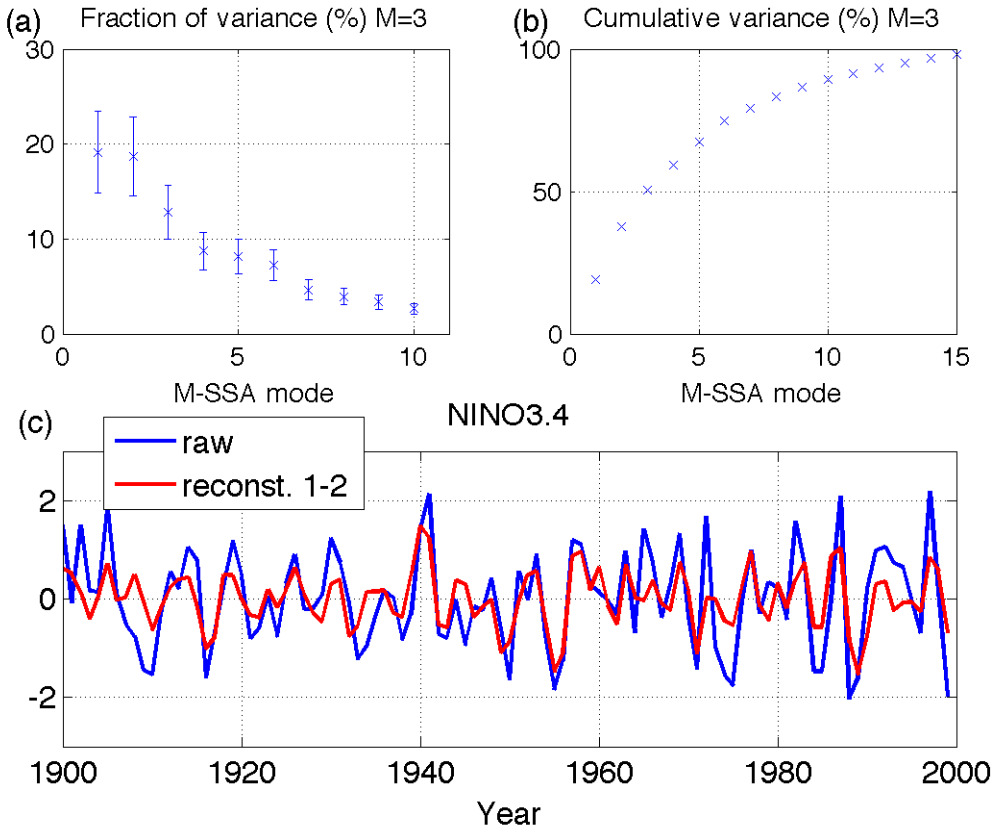

Fig. 7. M-SSA spectrum of the Pacific-centered multi-index set consisting of interdecadal anomalies (Fig. 6, red lines) of PNA, WP, NINO3.4, NPO, PDO, ALPI indices. The bottom panel shows raw time series of the NINO3.4 index and its RC based on M-SSA modes 1 and 2.

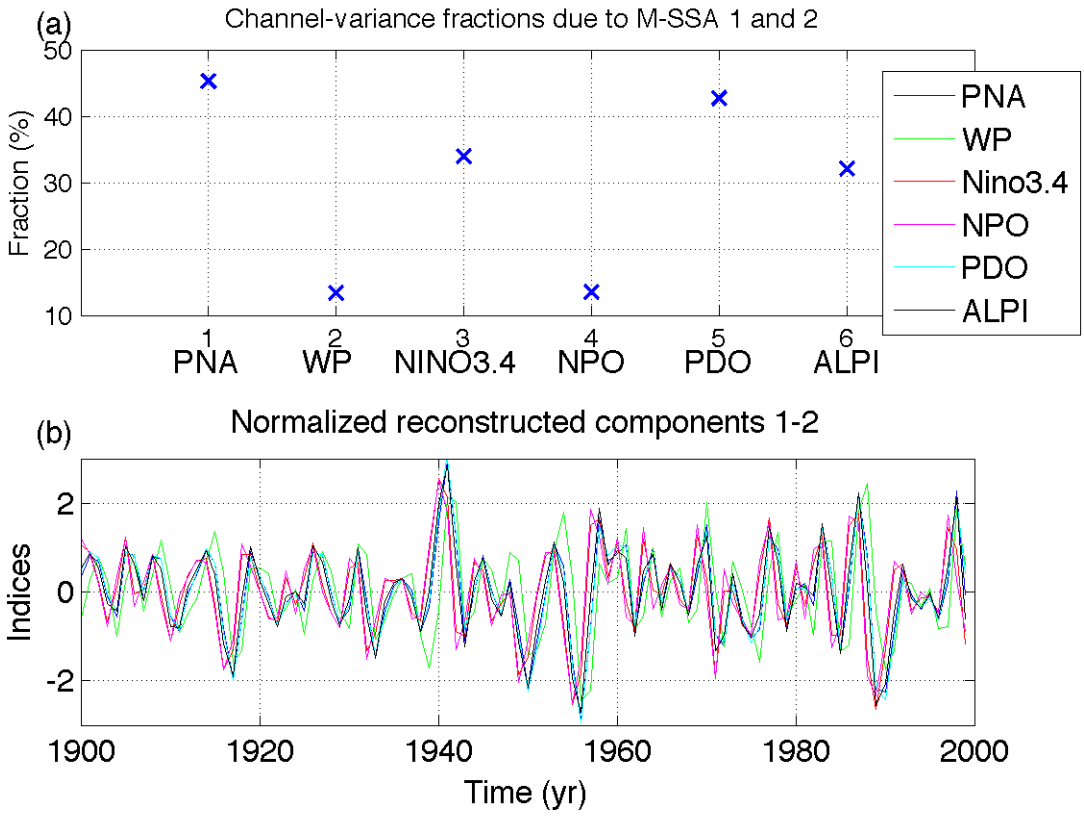

Fig. 8. The M-SSA results for the Pacific-centered index subset (see Fig. 7). See panel legend for abbreviated index names. Same conventions as in Fig. 5.

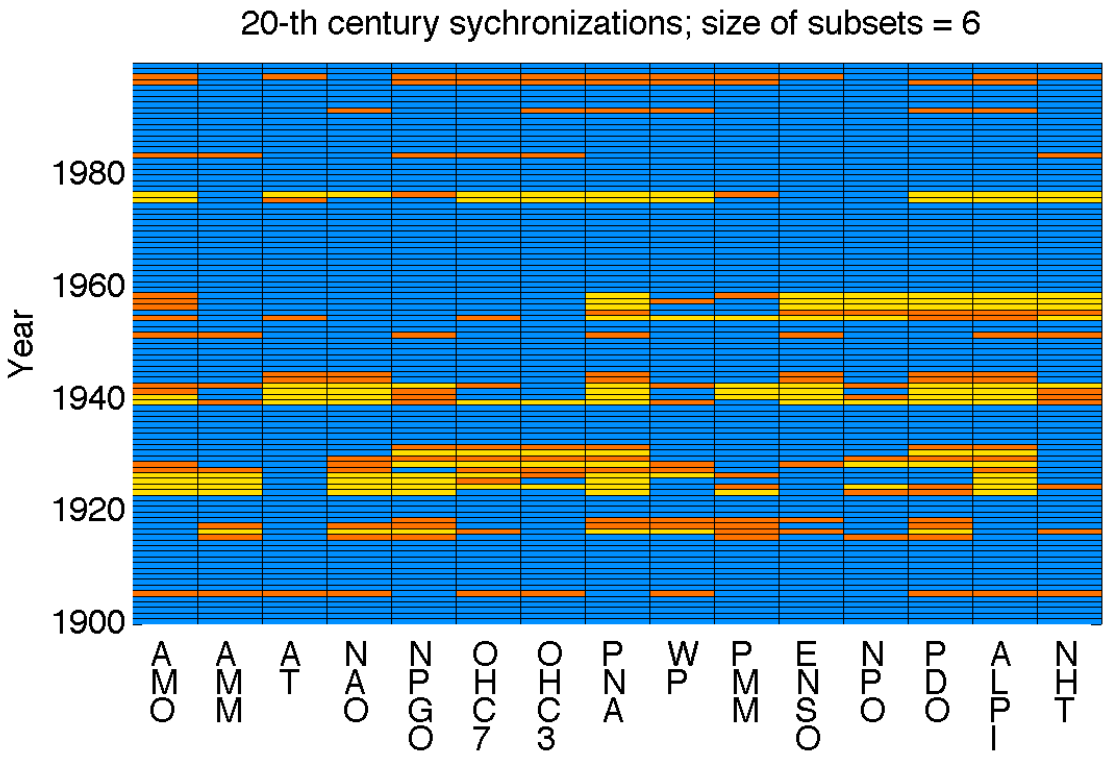

Fig. 9. Identification of index sub-networks. For a given year (on the vertical axis), bright yellow and orange cells indicate that there exists at least one six-index network that includes the index this cell represents (the indices are arranged along the horizontal axis), which is characterized by the network connectivity exceeding the 95th percentile of the connectivity for *all possible* 6-index networks and for *all years*; the yellow cells are characterized by the connectivity that exceeds the 99th percentile. See caption to Fig. 10 and text for the definition of network connectivity. The results for the subset sizes in the range from 4 to 8 (not shown) are analogous.

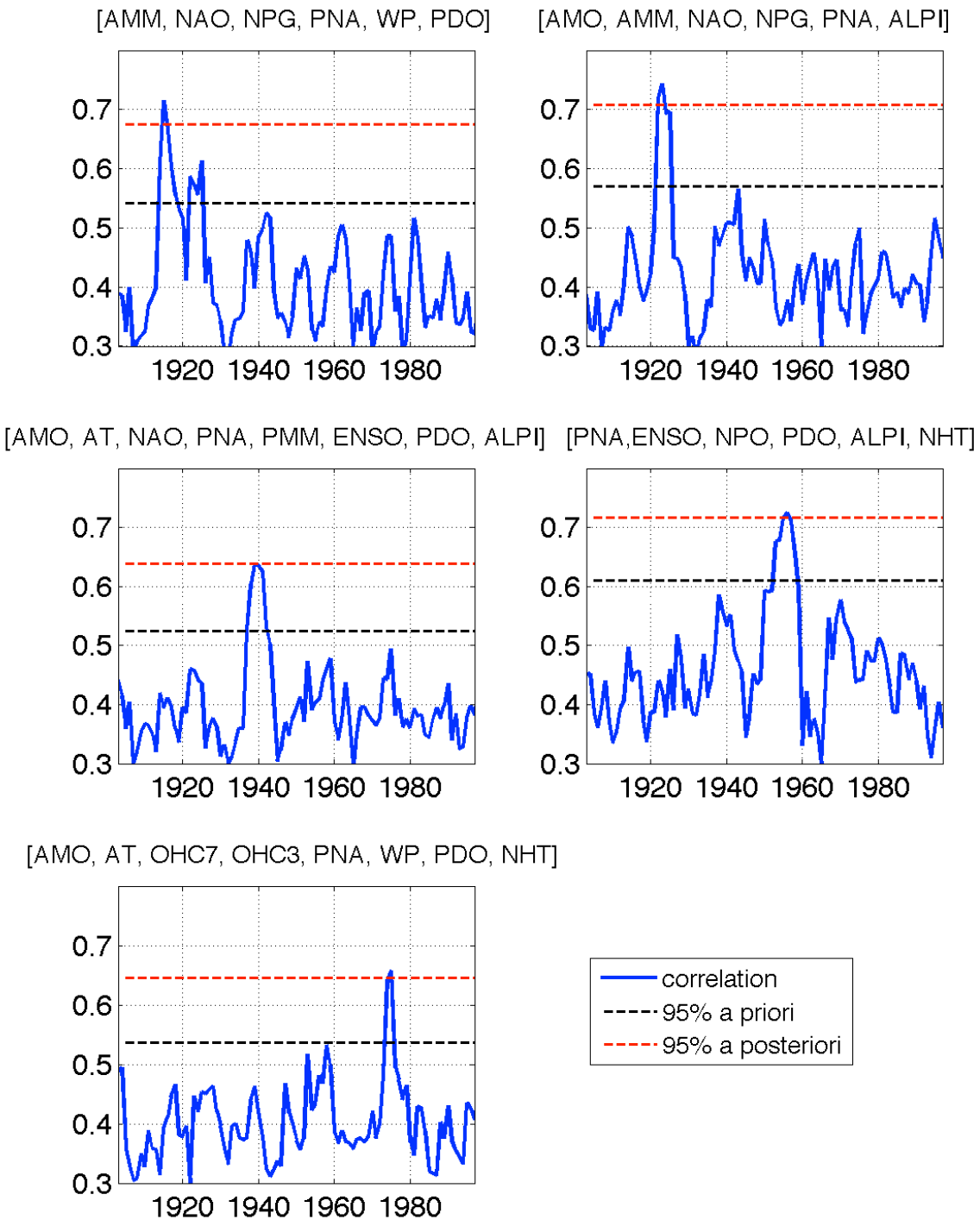

Fig. 10. The time series of index connectivity for the sub-networks identified in Fig. 9. The indices comprising each subset are listed in the caption of each panel. The measure of connectivity used here is the leading singular value of the lower triangular part of the index cross-correlation matrices computed over the 7-yr sliding window. The horizontal dashed lines indicate 5% a priori and a posteriori confidence levels based on the linear stochastic model that reproduces the *climatological* cross-correlations between the indices.

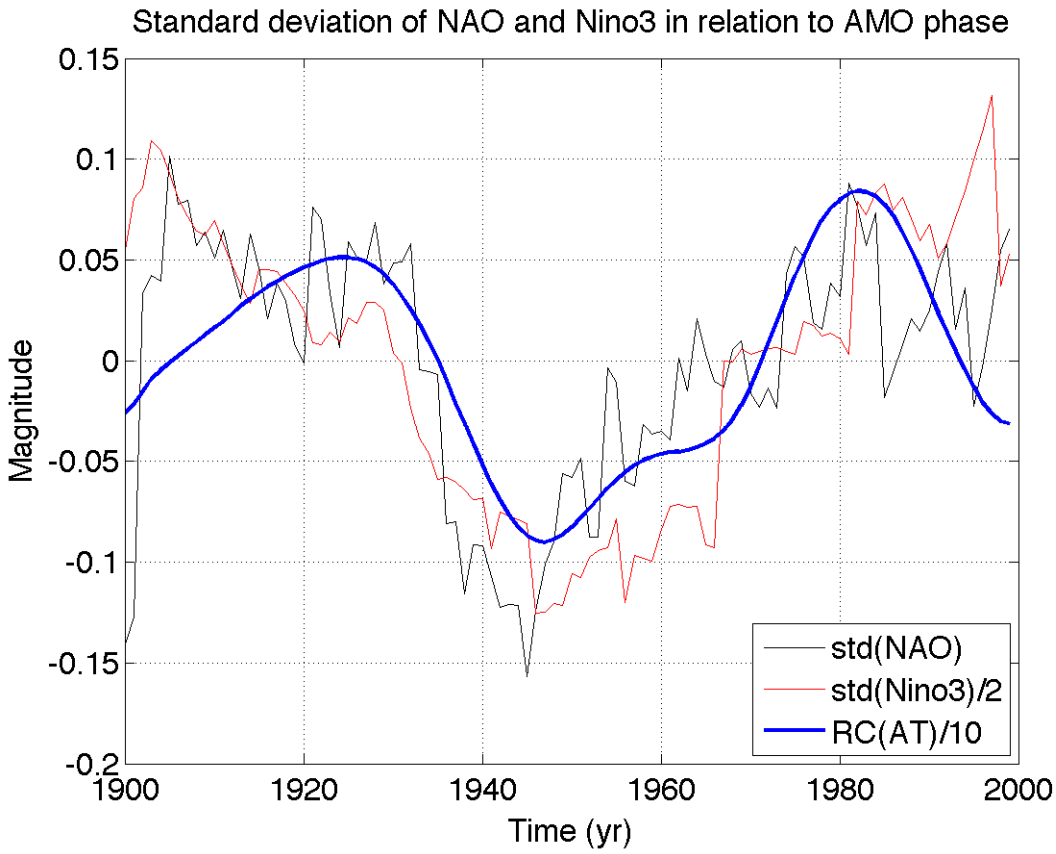

Fig. 11. Anomalies (with respect to the mean value of 1) of NAO (light black line) and Nino3 (light red line) standard deviations, along with the M-SSA mode's 1–2 RC of AT index (heavy blue line; this line is the same as that in the middle panel of Fig. 7, but multiplied here by a factor of 0.1). The Nino3 standard-deviation anomaly has been scaled by a factor of 0.5 for easier visual analysis. The standard deviations for each index shown were computed over the 31-yr-wide sliding window.